The Offshore Environment

Lucy Cradden, Pauline Laporte Weywada and Mairéad Atcheson

An accurate assessment of the offshore environment, including the meteorological, oceanographic and other relevant environmental conditions, is fundamental to the design of FOWTs. Using this information, the environmental loads acting on a device may be estimated, and the behaviour of a structure subject to these loads for both operational and extreme events can be predicted.

The characterisation of the offshore environmental and the creation of a metocean design basis for projects involving FOWTs will necessarily cover the site's offshore wind resource, the local wave climate and other key parameters such currents. All of these aspects are reviewed in detailed in Sects. 1–3 (respectively), where a brief description of the physics associated with each type of environmental input is presented alongside details on how to measure and map the resources.

L. Cradden
School of Earth Sciences, Energy Institute, University College Dublin, Dublin, Ireland
e-mail: lucy.cradden@ucd.ie

P.L. Weywada · M. Atcheson (✉)
Cruz Atcheson Consulting Engineers Lda, Lisbon, Portugal
e-mail: Mairead.atcheson@cruzatcheson.com

P.L. Weywada
e-mail: pauline.laporte-weywada@cruzatcheson.com

J. Cruz and M. Atcheson (eds.), *Floating Offshore Wind Energy*,
Green Energy and Technology, DOI 10.1007/978-3-319-29398-1_2

1 Offshore Wind Resource

Lucy Cradden

1.1 Origins of the Resource

The Origins of Wind

Wind energy is an indirect form of solar energy caused by the heating of the earth's surface by the sun. As the air above the surface absorbs the heat, it expands and the pressure falls. This lower density parcel of warm air then tends to rise. Cool air has a higher pressure due to its higher density, and it therefore tends to sink. The process of heating is uneven over the surface of globe—the equator receives more heat than the poles due to the relative positions of the earth and the sun. Landmasses also tend to heat up and cool down more quickly than bodies of water. This uneven heat distribution means different air masses will have different temperatures and pressures on both a large and small scale. In order to try and restore equilibrium, air will then tend to move from areas of high pressure to those of low pressure, thereby creating wind.

Further movement is induced by the spinning of the planet. As the earth rotates on its own axis, the path along which the air is moving appears to deflect relative to the surface. This is known as the Coriolis effect and leads to winds appearing to veer to the right of their direction in the northern hemisphere, and to the left of their direction in the southern hemisphere. The effect is largest at the poles and minimal at the equator.

Global Wind Patterns

In general, air will tend to move from the high pressure, cold poles to the low pressure, warm equator. This movement away from the poles generates polar winds that turn due to the Coriolis effect, and thus tend to an easterly direction (blowing from the east). As the warm air at the equator is heated, it rises and spreads. As it spreads pole-wards, it cools, and begins to sink again at around a latitude of 30°, and the pressure increases. Some of it is then drawn back towards the equator, forming the 'trade winds'. Because of the Coriolis effect, the trade winds will tend to turn from a northerly (in the northern hemisphere) or southerly (in the southern hemisphere) direction (i.e. coming from the north or from the south) to blow parallel to the equator in an easterly direction (from the east). The air that continues to move towards the poles from 30° to 60° latitude forms what are known as the 'westerlies', as the Coriolis effect causes them to tend to curve and blow in a westerly direction. A schematic of the overall trend in global winds is shown in Fig. 1.

Winds High in the Atmosphere

The movement of any fluid over a surface will be affected by friction. At a point far above the surface of the earth, typically between 500 and 1000 m, the influence of friction on the air flow is diminished. At this point, when the Coriolis effect and the

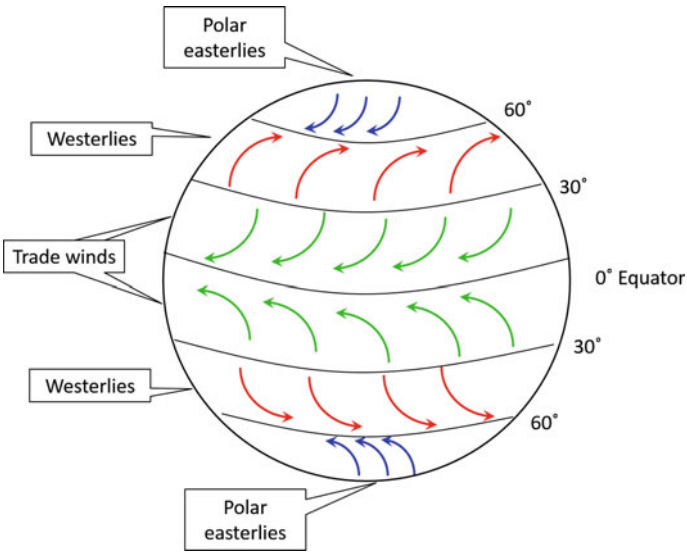

Fig. 1 Schematic diagram of global wind patterns (after Strahler and Strahler 1992)

pressure gradient are balanced, the wind will tend to blow in a direction perpendicular to the pressure gradient (i.e. following the isobars—lines of constant pressure), with the low pressure to its left in the northern hemisphere, and to its right in the southern hemisphere, as shown in Fig. 2 (Barry and Chorley 1998). The wind described solely by the balance between the influence of the pressure gradient and the Coriolis effect is known as the 'geostrophic wind'.

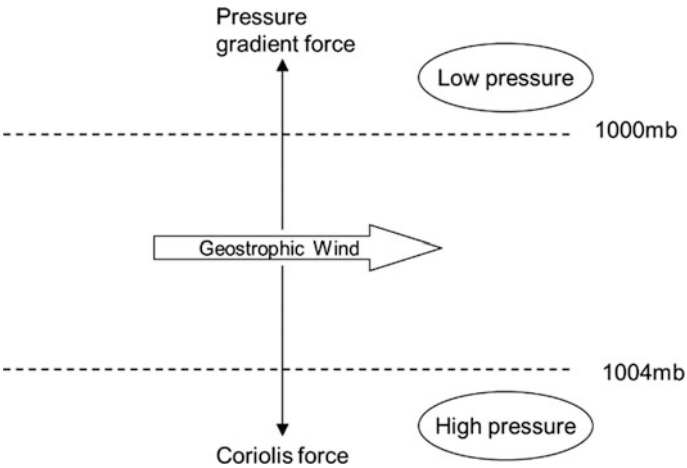

Fig. 2 Geostrophic balance in the northern hemisphere

The magnitude of the geostrophic wind, G, is given by:

$$G = \frac{1}{f\rho} \cdot \frac{dp}{dn} \tag{1}$$

where f is the Coriolis parameter which varies with latitude, ρ is air density and $\frac{dp}{dn}$ is the mean sea level pressure gradient. If the mean sea level pressure pattern for a region is known, it is possible to calculate the geostrophic wind velocity, which is representative of a hypothetical wind with no interaction with the surface. In actual fact, isobars are very often not parallel but circular, forming around a low or high pressure centre, and this leads to an additional centripetal acceleration. Balanced flow will be achieved in this situation with winds rotating anticlockwise around a low pressure centre in the northern hemisphere and clockwise around a high pressure centre (Barry and Chorley 1998). These winds are known as the gradient winds.

Localised Features of the Wind Resource

Geostrophic flow is only representative of wind conditions far above the earth's surface. In order to understand the wind velocity—and thus the available wind energy resource—at the height of a wind turbine, surface effects must be accounted for. The presence of obstacles, height changes and the wider characteristics of the terrain over which it is flowing can all influence the wind up to hundreds of metres from the surface.

Considering firstly the topography of the area in which the wind is blowing, account must be taken of the presence of hills, valleys, cliffs, ridges and other height changes in the surface. Coastal breezes are caused by the different heating and cooling patterns of the land and the sea. As the land heats up more rapidly than the sea during the day, the warm air onshore tends to rise and there is a drop in pressure. This draws in cooler, denser air from over the sea causing an onshore breeze. At night, the process reverses—with the land cooling down more quickly, the air above it sinks and moves towards the lower pressure areas over the sea, causing an offshore breeze (Strahler and Strahler 1992). Similar effects can occur around mountains and valleys—the air within a valley will heat up during daytime and tend to rise up the slope of the mountains, and as it cools over the mountain at night, will tend to sink back down into the valley.

The local wind flow will be directly disrupted by both smooth and abrupt changes in surface height causing, for instance, flow separation behind a steep drop, or speed-up over a hill (Troen et al. 1989). The nature of the effects on the flow will depend on atmospheric conditions and the wind speed itself (Stull 1988). Far offshore, obstacles or height changes are unlikely, but in coastal regions the physical presence of beaches and cliffs can exert a strong influence on the wind speed and direction. Additionally, individual obstacles near to a particular point of interest may have an effect on the wind experienced at that point. In an offshore setting, such obstacles could be the platform on which the measurement is being taken or perhaps the presence of local islands or a nearby coast.

Table 1 Standard roughness lengths assumed for different types of terrain (World Meteorological Organisation 2008)

Terrain description	z_0 (m)
Open sea, fetch at least 5 km	0.0002
Mud flats, snow; no vegetation, no obstacles	0.005
Open flat terrain; grass, few isolated obstacles	0.03
Low crops; occasional large obstacles, x/H > 20	0.10
High crops; scattered obstacles, 15 < x/H < 20	0.25
Parkland, bushes; numerous obstacles, x/H ≈ 10	0.5
Regular large obstacle coverage (suburb, forest)	1.0
City centre with high- and low-rise buildings	≥ 2

Another feature that affects the wind resource is the surface itself. When the air moves against the surface of the earth, its velocity is reduced due to friction with the ground. The magnitude of the frictional force is dependent on the characteristics of the particular surface in a location. These characteristics are summarised by the term *roughness length*, which is the theoretical height above a surface at which the effect of friction reduces the wind to zero velocity (American Meteorological Society 2015). Areas with a larger value of surface roughness will cause a greater reduction in the wind velocity and it will theoretically reach zero at a height further from the ground. Water typically has a lower characteristic surface roughness length than might be found onshore and is often given a constant value of 0.0002 m (see Table 1).

In reality, the roughness length at sea varies according to the impact of changes in wind speed on wave conditions, and is therefore not truly constant. The Charnock formula is often used to describe sea surface roughness, z_0, in the following form (Fairall et al. 1996; Lange et al. 2004),

$$z_0 = \alpha \frac{u_*^2}{g} \tag{2}$$

where α is a constant found from empirical measurements, u_* is the friction velocity (a measure of wind stress on the ocean) and g is acceleration due to gravity. The constant, α, is given a range of values in the literature, for example 0.0185 (Lange et al. 2004) and 0.012 (Peña et al. 2009).

The Charnock formula is generally applicable in fully-developed seas where the wind is blowing at reasonable strength over a large fetch but has been shown to break down in low wind conditions (Fairall et al. 1996). A number of extensions to the formula have been developed to account for the effects of different conditions on sea-surface roughness (Lange et al. 2004).

Vertical Profiles

The frictional and physical influences on the wind caused by the surface diminish with height above the surface, and the wind will generally increase in velocity with height. At some point far enough above the surface, normally between 500 and 1000 km, the wind will approach geostrophic conditions.

The effect of thermodynamics on the vertical air flow requires some additional consideration. As the ground is warmed by the sun during the daytime, the air above it is heated, and as it loses density the parcel of air will begin to rise upwards. Under what are known as *stable* conditions, as it rises, the air reaches a lower temperature than the surrounding air and will tend to fall back down again. A larger increase in wind speed with height is usually seen with a stable atmosphere. Under *unstable* conditions, the rising parcel of air cools but stays at a slightly higher temperature than the surrounding air and will continue to rise higher in the atmosphere. The change in wind speed with height will be lower than for stable conditions. The third condition is known as *neutral*, and in this case, the rising air maintains the same temperature as the surrounding air (Burton et al. 2001).

The change in wind speed with height above the surface is referred to as wind shear. Analysing the wind shear is an important part of a typical site assessment for wind for two main reasons—firstly, when taking measurements at a height that is not the hub height of the wind turbine, so that the measurements can be transposed to the correct height, and secondly when considering turbine design in order to consider loading across the turbine blades. Neutral conditions are perhaps most relevant, as they most often occur with strong winds and indicate a high degree of turbulent mixing (Burton et al. 2001). However, particularly at coastal locations, it is also important to understand the stable and unstable conditions.

In the absence of multiple measurements at a range of heights, theoretical wind profiles can be derived from measurements at one reference height. The wind speed, U, at a height above ground level, z, can be calculated for neutral stability using the following equation:

$$U = \frac{u_*}{\kappa}\left[ln\frac{z}{z_0}\right] \tag{3}$$

where u_* is the quantity known as *friction velocity* and represents the stress applied by the wind on the surface over which it is blowing, κ is the Von Karman constant and z_0 is the local surface roughness length. The derivation of this equation, known as the *log law*, is described in full in Manwell et al. (2009) and it requires a priori knowledge of the surface conditions at the measurement point. Using this equation and assuming that there are no obstacles or complex topography in the vicinity which will cause additional flow disruptions, wind speed U_{ref} measured at height z_{ref}, can be related to an unknown wind speed U at height z, using the following ratio:

$$\frac{U}{U_{ref}} = \frac{ln\frac{z}{z_0}}{ln\frac{z_{ref}}{z_0}} \tag{4}$$

where z_0 is the surface roughness length. For example, wind measurements taken at 10 m above the surface can be transposed to turbine hub-height. Accounting for

atmospheric stability requires the inclusion of an additional term in the equation derived from a principle called Monin-Obukhov theory, such that:

$$U = \frac{u_*}{\kappa}\left[ln\frac{z}{z_0} - \Psi_m\frac{z}{L}\right] \tag{5}$$

where$\Psi_m\frac{z}{L}$ is known as the *integrated stability function* and can be derived using various formulations (Lange et al. 2004). In stable conditions, the term z/L is positive and for unstable conditions it is negative. This modifies the ratio between the reference wind speed and the speed at the desired height as follows:

$$\frac{U}{U_{ref}} = \frac{ln\frac{z}{z_0} - \Psi_m\frac{z}{L}}{ln\frac{z_{ref}}{z_0} - \Psi_m\frac{z_{ref}}{L}} \tag{6}$$

The difference in the wind profile for neutral (log law only), stable and unstable (using Monin-Obukov correction) is shown in Fig. 3 using a roughness length of 0.0002 m, and where the 80 m wind speed is $\sim$10 m/s, following the calculation of Ψ_m as set out in Lange et al. (2004).

Another method frequently used to describe the vertical wind speed profile is the *power law*:

$$\frac{U}{U_{ref}} = \left(\frac{z}{z_{ref}}\right)^{\alpha} \tag{7}$$

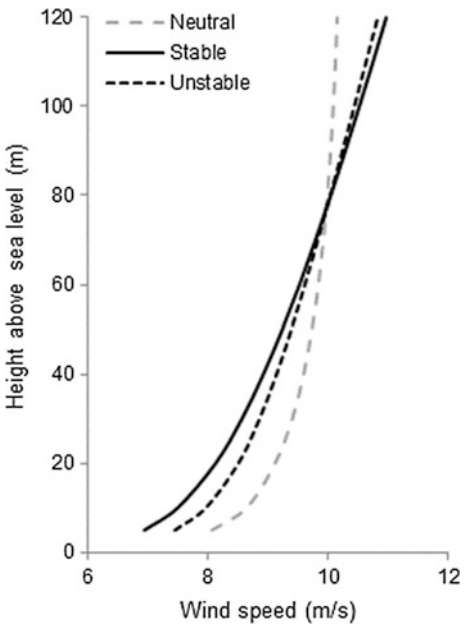

Fig. 3 Vertical profiles based on different stability conditions (after Petersen et al. 1998; Lange et al. 2004)

where α is referred to as the exponent, and is frequently assumed to have a value of 0.14 (Manwell et al. 2009; Petersen et al. 1998) or 0.2 (IEC 61400-1 2005). As both studies describe, the exponent can vary widely in reality, but the law is often used as a simple solution when data is not available.

Both the log law (with stability correction) and the power law have been found to incorporate error when applied offshore. Van Wijk et al. (1990) found that applying the Monin-Obukhov stability correction to the logarithmic profile assumption for locations in the North Sea improved the estimations of mean wind speed but with a degree of error remaining. Lange et al. (2004) found that for a site offshore to the south of Denmark, the Monin-Obukhov theory underestimated the increase in wind speed with height. Lange et al. (2004) suggests that the influence of the transition from land to sea in terms of the thermal effects can have an impact on wind conditions up to 100 km from the coastline, and application of a further correction to the Monin-Obukhov element can reduce the error. The author also indicates that the recommended standard assumption of 0.2 for the power law can lead to an underestimate in the wind shear. The difference in vertical profile for different exponents can be seen from Fig. 4.

Turbulence

Turbulence occurs on a number of scales within wind flow, induced by frictional and thermal effects. It can be seen as high frequency variations superimposed on a plot of measured mean hourly or half-hourly wind speeds, or as high frequency peaks in the analysis of wind power spectra. Generally, turbulent variations refer to scales of seconds and minutes, as opposed to variations that occur over hours and

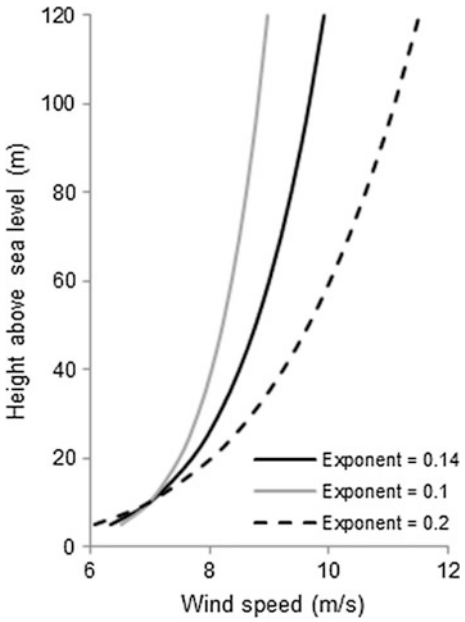

Fig. 4 Vertical profiles based on the power law with different exponents (after Lange et al. 2004)

days. The characterisation of turbulence at a site is a significant part of the International Electrotechnical Commission (IEC) design requirements (IEC 61400-3 2009). Turbulence is usually quantified at wind energy sites by the turbulence intensity, *TI*:

$$TI = \frac{\sigma}{U} \tag{8}$$

where σ is the standard deviation of the 10-min mean wind speed U. Measurements should be conducted at a high sampling rate ($\sim$1 min) for a sufficient period of time to capture a range of potential conditions.

For the case of offshore sites obtaining suitable measurements is potentially more difficult. Petersen et al. (1998) discuss the relationship between stability, surface roughness and turbulence, and give the *TI* for neutral conditions over the sea as being around 8 %, somewhat lower than for open grassland at 13 %. Hasager (2014) also discusses the relatively low ambient turbulence in the boundary layer above the sea compared to onshore locations. The IEC state that since the sea-surface roughness increases with wind speed, the turbulence will therefore also increase (IEC 61400-3 2009). In order to calculate *TI* for design purposes, the surface roughness length, z_0 found from an adaptation of the Charnock formula (by solving Eq. 3 for u_* and replacing in Eq. 2) can be used to calculate σ:

$$\sigma = \frac{U}{ln\frac{z}{z_0}} + 1.28 \times 1.44 \times I_{15} \tag{9}$$

where I_{15} is the expected value of turbulence at a wind speed of 15 m/s, with some reference values for particular turbine designs given in IEC 61400-1 2005. However, the IEC design criteria for offshore wind turbines (IEC 61400-3 2009) states that larger values of σ than those given as reference values, have been found offshore and this assumption is therefore somewhat uncertain.

Diurnal, Seasonal and Long-Term Trends

At a given point, the average wind conditions experienced will vary throughout the day, the season and from year-to-year. The diurnal variation pattern over land for mid-latitude regions such as Northern Europe is well-documented, and generally shows that the mean speed peaks around mid-day, and is minimum at night. This is due to thermal effects caused by the heating of the land by the sun, and thus the effect peaks in summer, but is minimal in winter (Manwell et al. 2009). In complex terrain, influences such as mountain and valley breezes can change this pattern. Offshore, less diurnal variation may be expected (Plate 1982) but studies suggest it is inconsistent: some work has identified little or no diurnal variation (e.g. Coelingh et al. 1996), whilst others (e.g. Barthelmie et al. 1996) have found considerable variability in the diurnal pattern, possibly depending on proximity to land.

Seasonally, wind conditions in northern Europe display a well-known pattern of higher mean wind speeds in autumn and winter, with lower speeds in spring and summer. Some differences in this pattern are apparent in the conditions across the

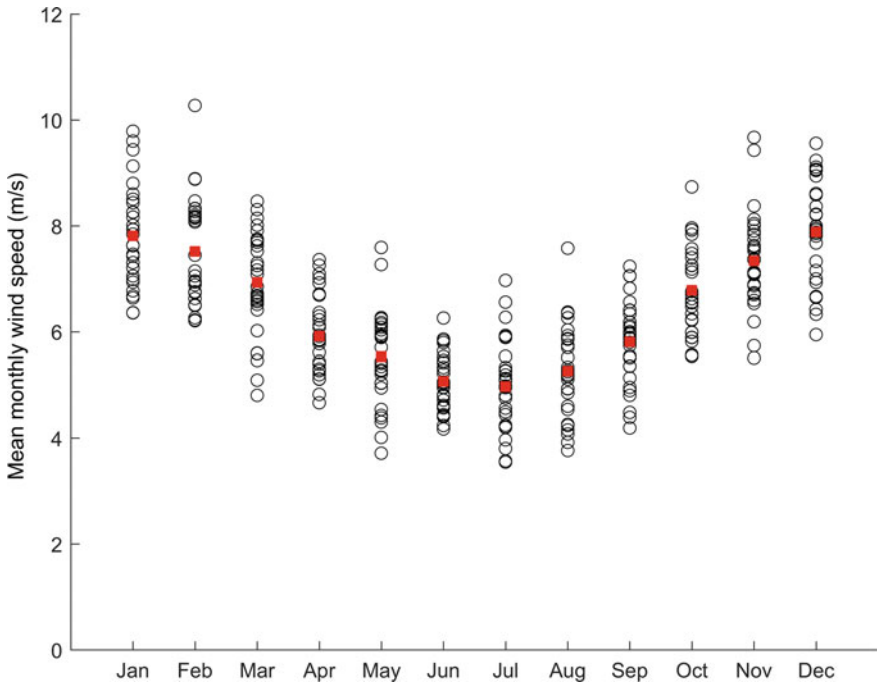

Fig. 5 Mean monthly wind speeds at a location off the coast of Cornwall from ERA-40 Reanalysis 1961–90

United States, as discussed in Manwell et al. (2009). Considerable variability can also be seen from year-to-year, and can also be significant inter-decadally. For the purposes of identifying long-term trends such as climate change influences (e.g. Pryor et al. 2005; Cradden et al. 2012), 30 years is considered to be the minimum period of study in order to capture normal inter-annual fluctuations. Figure 5 shows the monthly mean wind speeds for a 30-year period at a site off the south-west coast of England, using data taken from the ERA-40 Reanalysis (Uppala et al. 2005). The mean monthly pattern over the 30 years is shown by the filled dots, whilst each individual monthly mean is indicated by an open dot. There is a distinct, and expected, seasonal pattern but also considerable variability within the months from year to year.

Extremes

In the context of wind energy, it is critical to consider the design implications of the strongest wind conditions experienced at a site. Extreme winds are generally associated with storms, and are often defined by their *return period*, i.e. the period over which a certain level of wind speed could be expected to recur (Manwell et al. 2009). The IEC design criteria for offshore wind turbines (IEC 61400-3 2009) stipulate the requirement for the calculation of a 50-year extreme wind, which would be considered a reasonable design limit based on their expected 20–30-year

lifespan. It would be anticipated that due to the tendency for offshore winds to be higher, that offshore extreme wind speeds will also be relatively high compared to onshore. This has particular implications for turbine design and maintenance requirements.

Expected values for different return period wind speeds, where sufficient data are available, are generally found by statistical extrapolation of measurements. Using, say, 10 years of data to derive 50-year return period wind speeds can, however, incorporate uncertainty. The most widely applied method involves selecting a set of the highest occurring wind speeds in a time series (for example, the annual maxima) and fitting an appropriate distribution to these. Using the cumulative distribution function, $F(U_{annual\,maximum})$, the wind speed with a 50-year return period is that with an occurrence once every 50 years, or where $1 - F(U_{annual\,maximum}) = 1/50$ (Manwell et al. 2009). For a full explanation of methods used to select an appropriate set of extreme values and suitable distributions to fit to these, see Palutikof et al. (1999).

The IEC standard IEC 61400-1 (2005) recommends the assumption of values for the one year $V_{e,1}$ and 50-year $V_{e,50}$ return period wind speeds based on the following:

$$\mathrm{V_{e,50}(z)} = 1.4\mathrm{V_{ref}}\left(\frac{\mathrm{z}}{\mathrm{z_{hub}}}\right)^{0.11} \tag{10}$$

$$\mathrm{V_{e,1}(z)} = 0.8\mathrm{V_{e,50}(z)} \tag{11}$$

where z is the height at which the extreme value is being estimated, z_{hub} is the hub height of the turbine and V_{ref} is the reference wind speed provided by the turbine manufacturer and relates to the *class* of wind turbine into which the particular design fits (see IEC 61400-1 2005). Comparison of the statistical predictions and these values will help to inform the suitability of a turbine design for a particular location.

Considering specifically offshore wind turbines, combinations of extreme winds and extreme waves require additional analysis to understand maximum loads on the structure. The IEC indicates in IEC 61400-3 (2009) that it is unlikely that extreme winds and extreme waves will occur together, and for the purposes of design loads, extreme waves can be combined with a reduced version of the extreme winds.

1.2 Measuring the Resource

Typically, measurement of the wind resource involves recording the variation in time of the wind speed and direction at a single point, or several points spread throughout an area. It has traditionally been undertaken by national meteorological offices as part of their analysis of many weather parameters, but more recently, the

wind energy industry themselves have begun to establish new and bespoke measuring techniques for application to wind energy developments.

A number of different resource-related factors are important for determining whether a potential wind farm site is suitable for development and for analysing the more detailed requirements in terms of turbine design. Different factors may be investigated at different stages of a development, perhaps starting with a relatively low-resolution map of a region and moving on to more comprehensive measurements taken at a high temporal resolution at several locations around the site in question. When a promising site has been identified, further detail in terms of spatial and temporal variation is required, for instance to achieve the optimum farm layout—known as *micrositing*.

The electricity generation potential is, obviously, a critical factor in the wind resource assessment, as it underpins the financial viability of a development. The available wind power density, P, for a given cross-sectional area of flow, A, is a cubic function of wind speed, U:

$$\frac{P}{A} = 0.5 \times \rho \times U^3 \tag{12}$$

where ρ is the air density. A turbine can only extract a small amount of the available power, with the typical extraction characteristics being described by a *power curve*, such as that shown in Fig. 6. It can be seen that the turbine has a *cut-in* speed of around 3–4 m/s and reaches its maximum output at around 15 m/s, and additional speed above this value does not result in further power output. The turbine will cut out entirely to protect itself from damage at high speeds of around 25 m/s. For the purposes of power calculations, the relevant IEC standards (IEC 61400-1 2005; IEC 61400-3 2009) indicate a requirement for wind energy site assessments to be of the 10-min average wind speed, and this is usually sampled at hourly or half-hourly time steps. If possible, several years of measurements would be available in order to capture seasonal and inter-annual variations, but depending on the stage of project

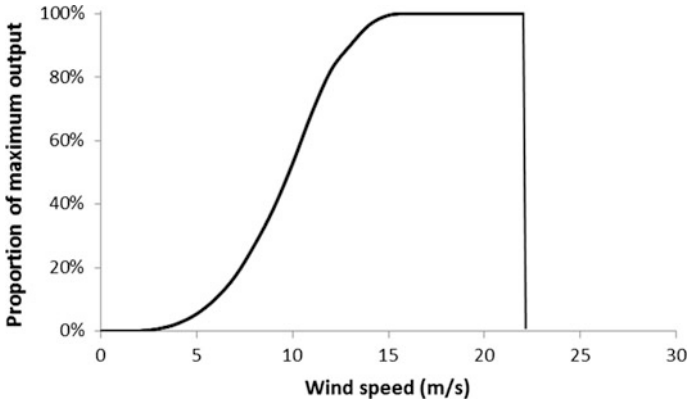

Fig. 6 Typical wind turbine power curve

development, shorter periods can be sufficient to estimate the site's potential, or additional modelling can be used to extrapolate the time series.

Traditional Anemometry

The technology used for measuring wind speeds at weather stations on land is usually based on a simple design using cup-shaped blades rotating around a central vertical axis, known as *cup anemometers*. The rotational speed of the cups around the central axis is proportional to the wind speed. A wind vane is generally used to record direction. Before the proliferation of wireless communication, measurements from anemometers were recorded manually on a form which was returned to a meteorological office, but newest stations record and transmit automatically.

Sonic anemometers work based on the time taken for a sound wave to travel between two points. A pair of transducers/receivers are set up opposite each other and each sends a sonic pulse towards the other. Based on the distance between them, the time taken for each pulse to be received at the other end can be used to derive the wind speed along that direction. Using several pairs of transducers at different orientations, the three components of wind velocity can be derived. Due to their ability to provide high frequency measurements over small distances (10^1 cm) these devices are particularly useful for characterising turbulence. The instruments are, however, sensitive to their positioning, which is particularly critical in non-horizontal terrain. In all cases, sonic anemometers will require careful calibration and post-processing (Wilczak et al. 2001).

Onshore, there are often large networks of weather stations including cup anemometers covering wide areas. For example, in the UK, the UK Met Office operates around 200 automatic weather stations each recording parameters including wind speeds at hourly time intervals and returning the information back to a central processing department (Met Office 2011). These records are held in a database for many years. Offshore, long-term measurements of weather parameters are often more sporadic due to the higher costs of installation and maintenance of measurement equipment at sea (Hasager 2014). Coastal and offshore wind speeds are traditionally recorded by lighthouses/lightships but in the past these may frequently have been estimated by observers rather than by using an instrument so the longer-term historical record may not be entirely robust. Networks of VOS (volunteer observing ships) exist that also record weather conditions and return the data to meteorological organisations, for example the Voluntary Observing Ships program in the United States (National Data Buoy Center 2014). The measurements, however, do not have a wide coverage. Meteorological buoys (met buoys) with anemometers on board are also deployed in specific locations in offshore waters providing, among other parameters, wind speed (and usually wind direction) measurements (see National Data Buoy Center 2015a for a map of buoys around the world). They return data in a similar way as onshore weather stations, via wireless communication networks to onshore data processing stations.

Measuring wind speeds at different heights is crucial to gain an understanding of vertical profiles (i.e. how the wind speed changes with distance from the surface), turbulence, and ultimately the potential for wind power generation and turbine design

requirements at a site. Met masts installed for the purposes of wind energy site evaluation can consist of several anemometers at different heights to capture the nature of the vertical profile under different conditions, and nowadays these often use sonic or ultrasonic anemometers alongside standard mechanical devices. Offshore, met masts of this type either require to be installed on a foundation which is fixed to the seabed, or on some kind of moored floating platform. It can be expensive to install such a foundation or platform and maintain the instrument in an offshore location.

In all cases, for accurate measurement of wind conditions, it is important that the anemometer is placed sufficiently high above surface level such that immediately local obstacles do not influence the wind speed being measured. Usually, in onshore cases, the masts are placed as far away as possible from trees, buildings etc. and are typically 10 m above ground level. The surrounding features need to be taken into account when interpreting the data. Offshore, achieving a constant height above surface level can be difficult as tidal fluctuations and waves can cause variations in the height of the water surface. Additionally, it depends on whether the platform on which the instrument is located is fixed or floating—for example it could be on a ship which is constantly in motion, or fixed to a seabed mounted pile which will not itself move. Taylor et al. (1999) discuss the issue of placement of anemometers on ships and the potential for interference from the vessel motion and structure on the measurements. Floating meteorological buoys that measure wind often do so at a height of around 2–3 m above sea level, which along with the motion of the buoy potentially introduces uncertainty to measurements, particularly in stormy conditions.

Some representative data has been obtained from the UK Met Office for wind speeds measured at the Sevenstones lightship moored off the south-west coast of England (Met Office 2006a). The anemometer is at 14 m above sea level (National Data Buoy Center 2015b) and the time period presented is 2014. The hourly sampled 10-min average time series of wind speed for the month of January 2014 is

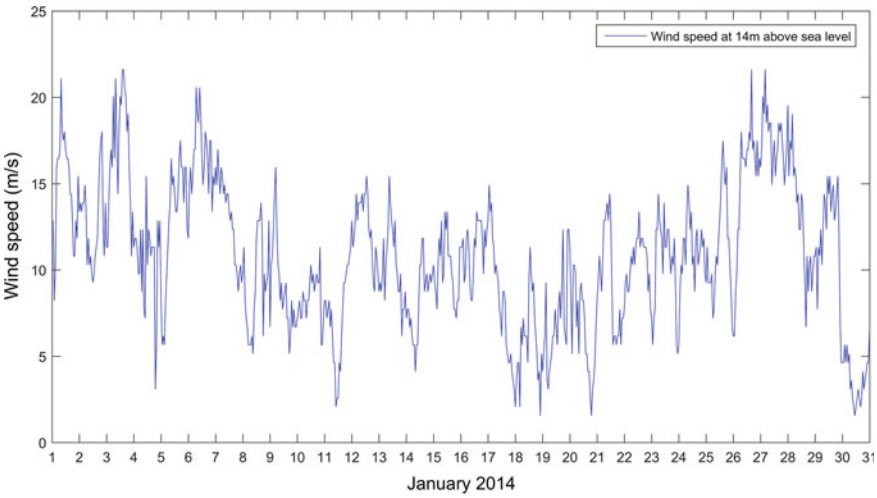

Fig. 7 Time series of wind speed at Sevenstones lightship (Jan 2014) (Met Office 2006a)

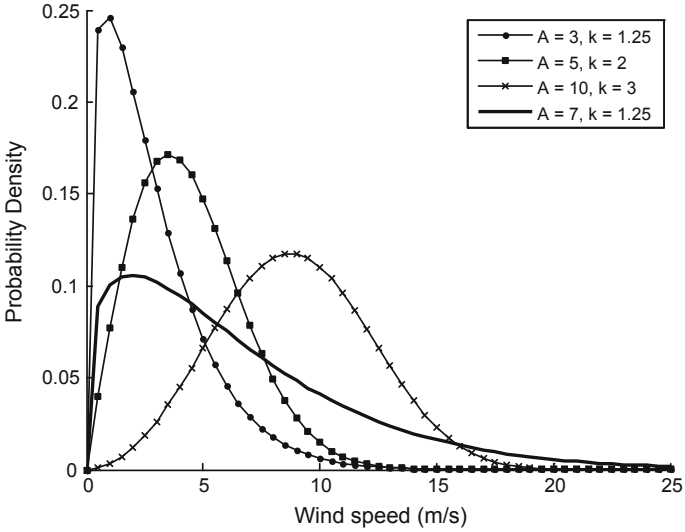

Fig. 8 Some shape and scale parameters for Weibull distributions

shown in Fig. 7. There is a large degree of hour-to-hour variation, which is generally present in these types of observation record.

Frequency Distribution

When carrying out a wind energy site assessment, the half-hourly or hourly measurements over a specific time period are usually summarised in the form of their frequency distribution. Wind speeds typically fit the pattern of a two-parameter Weibull distribution, as shown in Fig. 8, which can be described by two parameters, the *shape* and the *scale*. The scale parameter is related to the mean wind speed, whilst the shape parameter describes the variability of the wind speeds at the site—a lower shape parameter will have greater variability, with more frequent occurrences of high or low speeds, whilst a higher shape parameter indicates less variability. In the case of a site where a long period of hourly measurements is not available, the mean wind speed can be used to derive a Rayleigh distribution, which is a special case of the Weibull distribution, with a shape parameter fixed at a value of 2.

Combining the frequency distribution of wind speeds with the power curve will inform the developer of the expected energy output of a turbine at the site over the period measured, and thus the financial viability can be analysed. The distribution for Sevenstones is shown in Fig. 9, along with the fitted Weibull distribution with shape parameter 2.21 and scale parameter 9.99.

Direction

Analysis of the wind direction is a key feature of wind energy site assessments. Meteorological convention dictates that direction is expressed in terms of where the wind is blowing from (i.e. the opposite of the vector direction), and measuring in degrees clockwise from 0° at North. IEC 61400-3 (2009) specifies that directions

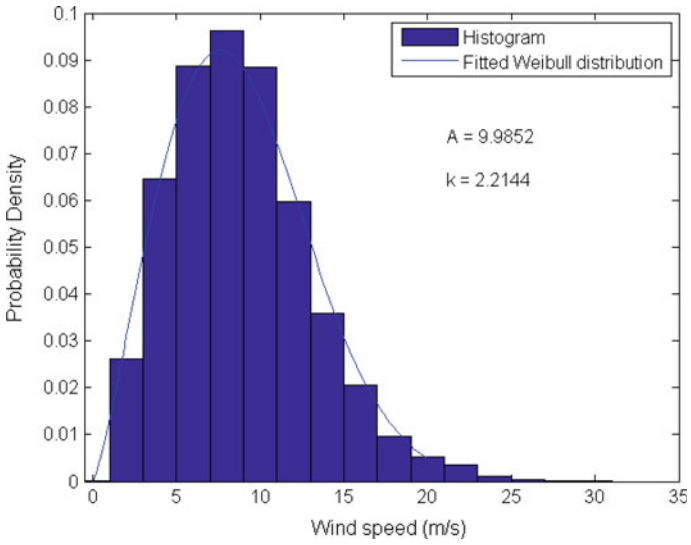

Fig. 9 Distribution of wind speeds at Sevenstones

are classified into sector bins with a maximum size of 30° for the purposes of creating a *wind rose*. Directional information may be required both for *micro-siting* considerations, including how to lay out the turbines within the wind farm and for turbine design and loading analysis.

Figure 10 shows the wind rose measured over a year at Sevenstones with sector bins of 10°. As would be expected, for this location a large proportion of the winds come from the west and south-west. At low speeds (dark blue), the directions are actually less heavily weighted to the west, but for wind speeds in peak range for generation (10–20 m/s), the majority of these occur in the western quadrants.

Remote Sensing

There is an increasing demand, somewhat driven by the wind energy industry, for alternatives to mechanical measurement systems, featuring the use of sound-waves, and more recently, laser beams to measure wind speeds. These can often be located some distance away from the site of interest, hence the term *remote* sensing. In the case of offshore wind developments, developers are interested in using these techniques at existing wind farms, locating devices temporarily on current infrastructure in order to better capture information about turbine wakes and wind profiles (Hasager et al. 2008).

Sodar (SOnic Detection And Ranging) systems work by sending out sonic pulses. As these beams meet turbulent structures in the atmosphere (eddies) they reflect a certain amount of the beam (backscatter). Due to the Doppler effect, if there is a change in frequency of the reflected wave, this indicates movement towards or away from the receiver along the axis of the beam. This way, the speed of the air movement can be determined. Lidar (LIght Detection And Ranging) wind measurement devices send out a laser beam, rather than a sound wave. When the beam

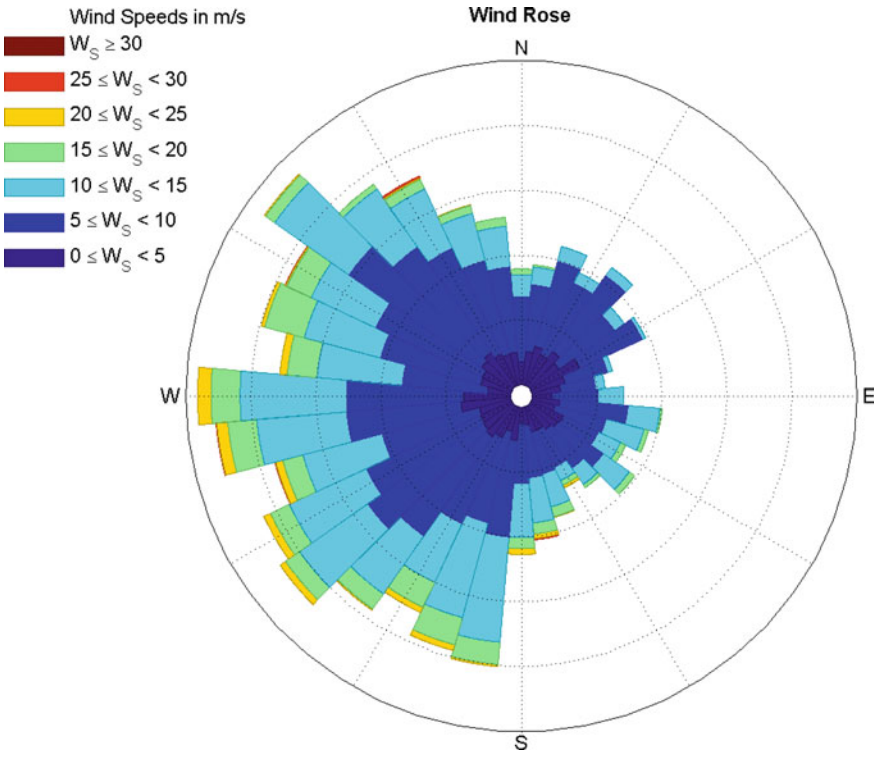

Fig. 10 Wind rose for Sevenstones

encounters particles in the air (pollen, dust etc.) the beam is scattered and some of the scattered light is reflected back towards the device (Smith et al. 2006). Again, due to the Doppler effect, the change in frequency of the reflected light can be used to determine the velocity of the particle along the beam axis. The device needs to scan in multiple directions to capture the full information on the wind velocity, and a post-processing algorithm is required to transform the information from the laser beam into wind velocity data.

Lidar is frequently used to analyse specific aspects of the wind field—for example, variations in speed across a turbine rotor, or in its wake, to map wind fields over a region in 2-dimensions, and to look in detail at vertical profiles (Peña et al. 2009). The technology can be expensive, but there are a number of proprietary devices developed by wind energy consultancies around the world that developers can rent or purchase (see Hasager et al. 2008). A significant proportion of their accuracy is dependent on the post-processing of the Doppler shift information into accurate wind velocity data, as well as the specifics of the laser technology involved. Cloud, mist and rain can all potentially introduce error into the wind speed measurements from Lidar (Smith et al. 2006). Det Norske Veritas (DNV) provide a recommended practice DNV-RP-J101 (2011) to operating and using data from remote sensing equipment, which states that the output should be verified against the

measurements from an in situ met mast, and that consideration of the positioning of the device is crucial to avoid interference from nearby obstacles, for example trees and buildings. The presence of particularly complex flow situations can also influence output and should be accounted for when analysing the results.

Satellites

In the case where a wider-scale picture of the offshore wind field is required rather than at a single point, there is an option to use data measured remotely from devices attached to satellites. The first instruments, deployed by NASA in the 1980s passively measured the microwave radiation associated with the roughness of the sea surface, and correlated this to the magnitude of the local wind speed (Hasager 2014). More recently, active devices called scatterometers are being used that emit and measure the backscatter of microwave radiation. The degree of backscatter in the microwaves along different axes caused by very small waves on the ocean surface (wavelengths on the order of centimetres) can be detected by the instrument. An algorithm is applied which relates the magnitude of the backscatter along the different axes to the local wind speed and direction as it blows over the ocean surface. The algorithms are developed and calibrated based on empirical relationships identified between the backscatter and either in situ measurements, model data or both (Sempreviva et al. 2008).

Satellites follow pre-determined tracks around the globe with the ability to take measurements covering areas around 2000 km wide as they pass, so each orbit gives good daily coverage of the whole earth. Several world-wide organisations are now responsible for operating satellite scatterometers, including NASA (RapidScat; NASA 2015), and EUMETSAT (Jason-2; EUMETSAT 2015). The frequency of travel of the satellite over a particular part of the ocean determines the time resolution of measurements, which can be between 2 and 6 times daily, with a spatial resolution typically in tens of kilometres. Where higher spatial resolution is required, an instrument called a SAR (synthetic aperture radar) can be used instead of a scatterometer. This emits a single microwave beam directly perpendicular to the sea surface and from the backscatter, the localised wind speed can be determined. SAR measurements are typically available at lower frequency than scatterometers (perhaps a few times per month) but at a much higher resolution of 10^1 m (Hasager et al. 2006; Sempreviva et al. 2008).

For all types of satellite technology, the accuracy of the algorithm used to interpret the backscatter signal and relate it to the local wind conditions is key to the accuracy of the data. Further processing is required to map the measurements taken from each pass of a satellite over an area of ocean onto a regular grid covering the region of interest. In coastal regions, there is often a lot of interference from the land, so measurements using scatterometers here tend to be unsuccessful, whilst for some types of scatterometer, the presence of raindrops will also adversely affect the accuracy of measurements (Weissman et al. 2002). Hasager et al. (2006) indicates that SAR is generally considered to be more useful for coastal measurements and also demonstrates that SAR measurements are sufficiently detailed to capture the wake effects from an offshore wind farm.

1.3 Resource Mapping

Obtaining information about spatial variations in wind conditions over a specific area requires some degree of modelling to *fill in the gaps* where measurements are not available. For instance, a wind farm developer may wish to find the site with the best resource in a particular area, but measurements are only available from one point within the area, or policy-makers may wish to map the resources for their whole region, but again, only measurements from specific points within the region are available. As previously mentioned, in the case of offshore wind existing measurements are particularly rare, and thus modelling offers a reasonable alternative. Different modelling techniques are appropriate for modelling at different scales, and for different applications depending on the accuracy and resolution requirements.

Statistical Models

With growing interest in the wind industry in the 1990s, but at a point where computing power was still very limited compared with what we are familiar with today, the use of statistical models to relate wind speeds measured at one location to those experienced at another location of interest was prevalent. A technique known as Measure-Correlate-Predict (MCP) was (and often still is) widely used to develop a relationship between winds measured over a short period at a specific site of interest for wind energy development and longer-term measurements—perhaps 3–10 years—from a nearby location. This allows the characteristics of the longer time period to be taken into account when considering the energy potential or design requirements at the proposed site. A number of different software packages exist that apply MCP techniques.

Given a location, *A*, with a long record of wind speeds and a second location, *B*, with a shorter period of records (which overlaps with some of the period of the *A* record), the fundamental process involves firstly *binning* each set of wind speed measurements by directional sector. For the short period in which the measurements overlap, a relationship is found between the two sets of wind speeds in each directional sector. The relationship is commonly derived using simple linear regression, but it can also involve relating the parameters of the fitted Weibull distributions, or other more complex methods such as neural networks (Carta et al. 2013). This relationship is then applied to the wind speeds from site *A* to derive corresponding *measurements* for site *B* and extrapolate its short record to cover the longer period of the *A* record. Where the terrain is smooth between the two sites, with no complex features such as mountains to drastically alter the flow, this technique is usually successful. In the case of more complex topography, however, the relationships can carry a larger degree of variability, and thus the associated uncertainty can be higher.

Going from an onshore site *A* to an offshore site *B* is an example of where such uncertainty might be found, as the coastal processes and the change in flow as the wind goes from on—to offshore or vice versa will introduce complexity that may not be fully represented by a statistical relationship. By way of demonstration, two

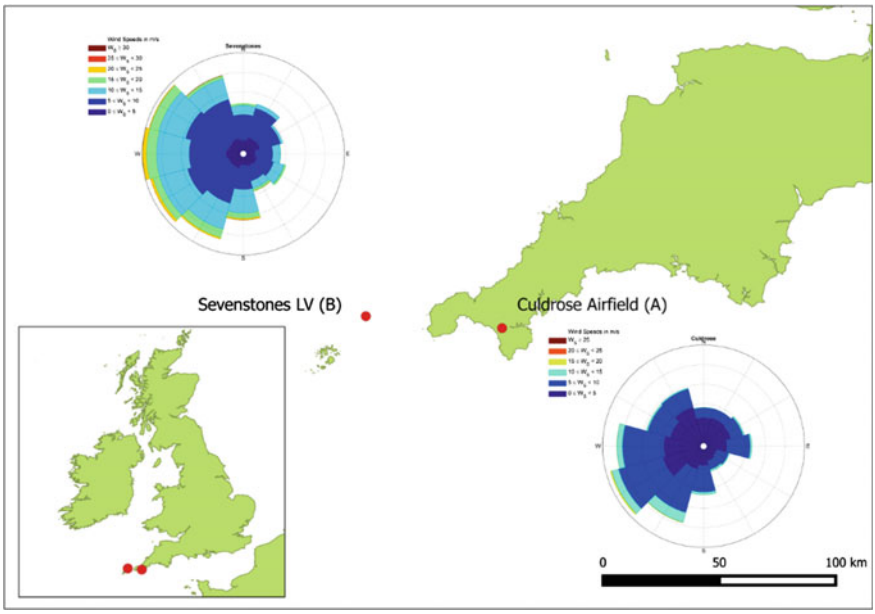

Fig. 11 Site locations and wind roses used in the MCP example

sets of recorded wind speeds have been obtained, one from an onshore weather station (Met Office 2006b) and one from a light ship moored approximately 60 km away (Met Office 2006a). The record covers the year 2014, so has been initially divided in two, so that the first 6 months can be used to develop a simple linear relationship between wind speeds at each site, and the second 6 months of offshore wind will then be predicted using the second 6 months of onshore records. The predictions can then be compared to what actually occurred to assess the degree of error in the method. A map of the two sites and the associated wind roses from the two met masts is shown in Fig. 11.

At each time step, the data from both sites was binned according to the direction occurring at site *A*, Culdrose, and for each directional bin, a regression was carried out with the two sets of wind speeds to fit a simple linear relationship between the occurrences at each site. The *R*-squared correlation coefficients for the overall six-month period was 0.68, and Pramod Jain (2011) suggests that a correlation coefficient of >0.65 for two sets of 10-min average wind data is sufficient to proceed with a MCP analysis. Individual *R*-squared coefficients for each bin were quite varied, with those in bins from the south-southeast to west showing *R*-squared values of 0.7–0.9, whilst for winds coming from the north and east, the *R*-squared values were only around 0.4–0.6. Considering the locations on the map, this would correlate to the fact that both sites are similarly exposed to the south and south-west, whilst for winds from the north and east, the terrain and topography are quite significantly different at the two sites. Other authors, as discussed in Carta et al.

(2013), indicate a requirement for a greater correlation between the two sites and in this case, it would be considered that the uncertainty may be quite high. The fact that seasonal variation may not be adequately captured within the 6-months of concurrent data may also be a contributing factor.

The regression coefficients have been used to derive the second 6-month period of wind data for the offshore location from the onshore record. Comparing the predicted and actual offshore values for the 6 months predicted, the overall *R*-squared value is around 0.6, indicating a not insignificant difference. Using the original and predicted data to calculate the wind power output using a standard power curve shows that the MCP method under-predicts the production for those 6 months by around 4 %. This may indicate that the wind speed distribution is reasonably well captured but the time-sequence is not so successful. Therefore, care must be taken when using statistical methods to ensure that they are robustly applied and that the error is sufficiently understood.

Micro-Scale Modelling

Micro-scale models are, as the name might suggest, used when dealing with relatively small spatial scales. A solution which builds upon the premise of relating wind measured at one site to another nearby site was developed in the 1990s and is known as the Wind Atlas Methodology. This is a physical model, rather than a statistically-based solution, and forms the basis for a well-known piece of wind analysis software, Wind Atlas Analysis and Application Program (WAsP). The method and its application to mapping the wind climate of Europe is described in great detail in Troen et al. (1989). The model attempts to capture the effects of three main influences on wind speed: local obstacles such as buildings, the general surface conditions (see Table 1) and the topography, which refers to height changes in the terrain such as hills or cliffs. The premise behind the Wind Atlas Methodology is that given a measurement at a point within a region and a description of the surrounding location, the known influence of all three categories can be removed from the initial record, leaving a representation of a more general regional wind climate. For a point of interest within the region at which no measurements are available, the influence of particular local features at this new point can be added back into the regional climatology to provide a representative record here.

A key advantage of the Wind Atlas Methodology is that it requires relatively low computational effort, but it does neglect non-linear influences on local wind conditions. This makes it less successful in very complex terrain, such as mountainous areas. In an example situation of a resource assessment for a coastal location on an island above quite steep cliffs and nearby to a mountainous area, the WAsP model was identified as being invalid due to an established inability to capture these local effects (Palma et al. 2008). WAsP assumes a constant surface roughness of 0.0002 m over water, rather than the more complex assumption whereby z_0 varies with wind speed. It also makes some simplified assumptions about heat flux, which inform the stability conditions in the model (Lange and Højstrup 2001). The use of WAsP offshore was studied in Lange and Højstrup (2001), which indicated that

whilst mostly successful, a combination of the assumptions in the model do cause some errors in wind power estimates compared to reference measurements. Longer fetches appear to show under-prediction and shorter fetches over-prediction of the resource.

As computing power and confidence in the modelling techniques increase, non-linear models show much greater accuracy in complex situations than simpler statistical and wind atlas type methods. Computational Fluid Dynamics (CFD) typically use Reynolds-averaged Navier-Stokes (RANS) equations to model the fluid (i.e. air) motion in a locality as it interacts with obstacles and terrain features. Non-linear effects are included in these models but the computational effort required is substantially more than that for a linear flow model. Some bespoke software has been developed specifically for wind energy purposes, but more generally applicable CFD models can be set up for a wide range of fluids and environments and can thus also be used to carry out wind modelling. The use of these kinds of models require extensive verification and validation, for example using wind tunnels (Ayotte 2008), to ensure that they are truly representative of the situation they are modelling and to understand their sensitivities and uncertainties. In Palma et al. (2008), the use of CFD alongside a number of anemometers showed good comparisons with the measurements and also allowed features such as flow separation and turbulence intensities at the proposed development sites to be mapped to a high resolution.

Mesoscale Models

Mesoscale model is a term widely used to describe numerical weather prediction models that have the ability to resolve weather features that are on a scale of 10^1–10^2 of kilometres. Solving equations representing atmospheric physics and dynamics, the models can calculate parameters including air temperature, pressure, density and velocity. They are used in both forecasting and hindcasting mode, to predict incoming weather or reanalyse historical weather. Their operation is similar in either case, but for hindcasting, instead of propagating a known situation forwards, they are propagated backwards in time, and constrained by known boundary conditions measured throughout the time period of the hindcast to reproduce a representative historical climate. For wind power applications, these models are typically used when information is needed on wind speeds over wide areas, such as a state or country. Their scale and computational demand is such that they are typically set to produce wind conditions averaged over grid cells between 3 and 50 km length.

Generally, the models produce time series of wind vectors (or wind speed and direction)—for example, hourly—in gridded format. Whilst the output is expected to be representative of the climate throughout the grid cell in question, it may not be an exact match for the wind speeds at any given specific point within the cell, particularly if the terrain varies widely within the cell. Their main benefit is in providing a way to look cumulatively at the wind climate for an area, how it varies within the wider area, and perhaps to model aggregate wind power output over this area (see for example Harrison et al. 2015).

As discussed in Watson and Hughes (2014), the models do not always capture the finer details of the offshore resource as might be relevant in a more localised energy potential assessment, for example the directional changes and stability conditions at a site. The authors found greater accuracy compared with met mast data further offshore than close to the coast, indicating that as with most other types of model, capturing the land-sea interactions is problematic. Their output can, however, be used as input to finer-scale models, such as those using CFD, which can apply the influence of more localised conditions. Mesoscale models can also be used as input conditions to wave forecast/hindcast models and can potentially be used in this way to look at concurrent wind and wave loading conditions for offshore wind developments.

Examining some output from a 10-year simulation at 3 km spatial resolution around the UK and Ireland of the WRF (Weather Research and Forecasting—Skamarock et al. 2008) mesoscale model (Hawkins 2012), firstly it can be noted that the areas with highest wind speeds in this region can be seen to the west and north west and to a lesser extent in the northern North Sea area (Fig. 12). Secondly, clearly the spatial variability of the offshore wind conditions is much less than

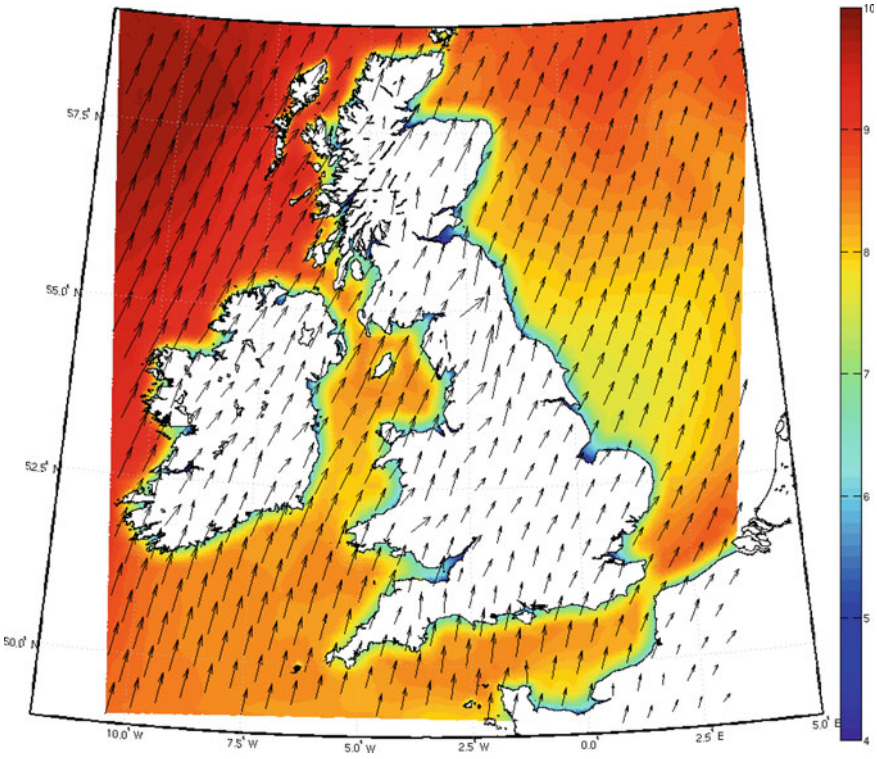

Fig. 12 Mean 10 m wind speed from WRF mesoscale model at 3 km resolution from 2001 to 2010

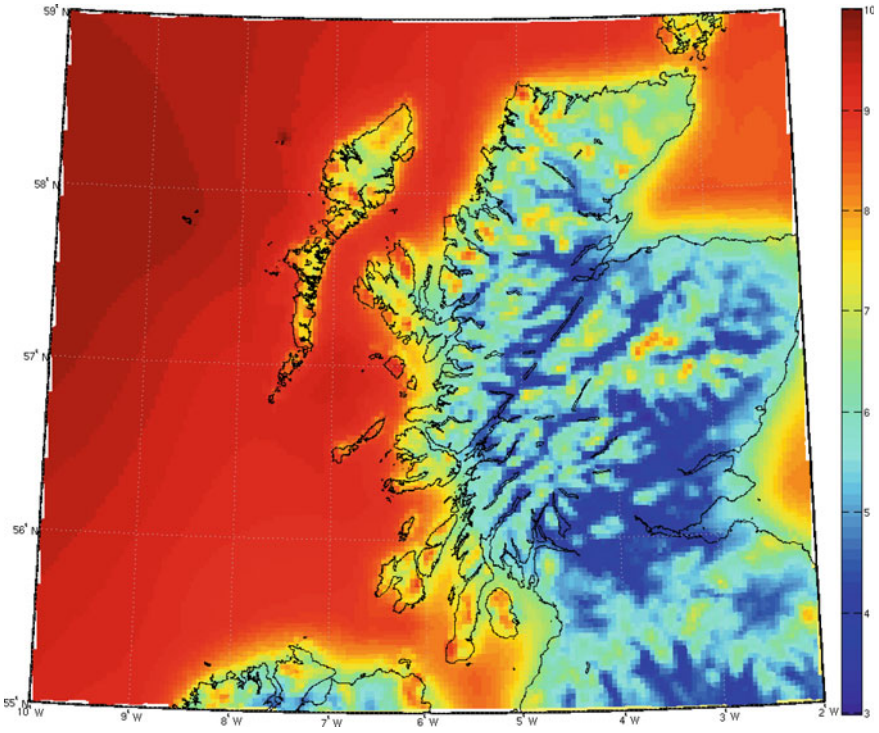

Fig. 13 Close-up of Scotland showing differences in the spatial variability of wind speeds for onshore and offshore

would be found onshore, as the surface conditions are much more consistent. This gives rise to smooth contours of mean wind speed across swathes of ocean and reasonably consistent directional patterns over wide areas of ocean, since there are no large obstacles or terrain height variations, the larger-scale climate features are the predominant influence. This is highlighted in Fig. 13, showing the difference in spatial variations on- and offshore, and is explored further in Cradden et al. (2014), where it is also demonstrated that, for a given location, hourly wind speeds from the hindcast are less variable offshore than at locations with complex terrain onshore. Coastal wind velocities are usually 10–20 % lower than the areas further offshore which is borne out by the model output shown here (Barry and Chorley 1998).

The theoretical capacity factor of a generic 3 MW wind turbine has been calculated using the 80 m wind speeds extracted from the WRF model output for 2010 and is shown in Fig. 14. Generally following the pattern of the 10 m wind speeds, the highest capacity factors are found in the west and north west of the map. The water depth in this region, however, increases very steeply moving out from the coast and the resource is only likely to be exploitable using floating turbine platforms rather than fixed foundations. For the region to the west of the English Channel where the resource is also promising, the water depth is much more

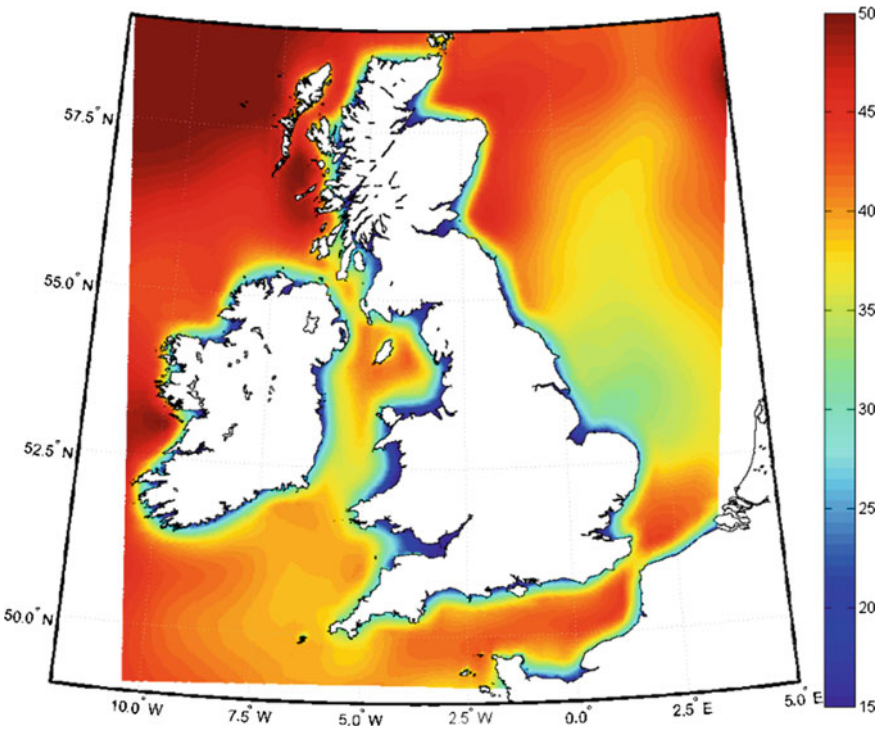

Fig. 14 Hypothetical capacity factor for a generic wind turbine using 80 m wind speeds extracted from WRF for the year 2010

shallow and fixed foundations are suitable. In the areas of the North Sea to the east of Scotland, the water depth is quite variable but can reach the limit of the newer fixed foundations, making floating platforms a viable option here also.

Global Wind Resource Maps

Maps of wind speeds around the world give an overall picture of where the most significant resources are located. A typical source of input data for such maps is either satellite records (Hasager et al. 2006; Risien and Chelton 2006; Hasager 2014) or alternatively using the reanalysis datasets. Reanalysis data have been created by several meteorological organisations around the world by running numerical weather prediction models in hindcast mode for several decades, with recorded observations included in the simulation to constrain the model with real data. Examples of reanalysis projects include ERA-40 (Uppala et al. 2005), its successor ERA-Interim (Dee et al. 2011) and NCEP-CFSR (Saha et al. 2010). The maps in this section have been generated using the MERRA reanalysis which uses satellite information recorded since 1979 assimilated into a global circulation model (Rienecker et al. 2011). The data covers almost all of the offshore areas of the world

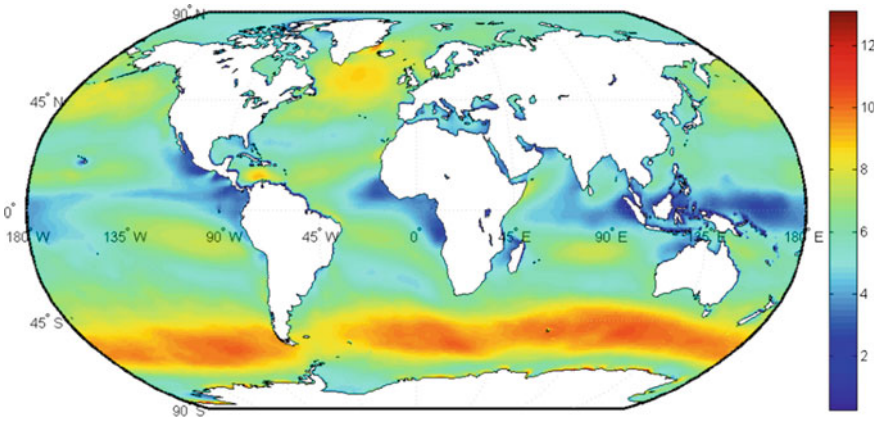

Fig. 15 MERRA mean annual surface level wind speed (2014)

at a resolution 0.5° latitude by 0.667° longitude. It is freely available for download from (Goddard Earth Sciences Data and Information Services Center 2013).

The average wind speed at 10 m above sea level (a.s.l) for the year 2014 is shown in Fig. 15 and the mean annual wind power density is shown in Fig. 16. The area known as the *doldrums* is quite evident around the equator, with the trade winds in each hemisphere appearing as the green-yellow zones above and below this area. The peaks around the areas of 45° north and south of the equator are the westerlies. These tend to be somewhat weaker in the northern hemisphere due to the larger land mass. The seasonal variation in wind speeds during 2014 can be seen to some extent in Fig. 17, which shows mean 10 m a.s.l wind speeds for December and July. It is clear that the northern Atlantic and Pacific Ocean regions see a large difference between the summer and winter wind speeds, whilst the regions around the Indian Ocean and the Arabian sea, for instance, show the opposite trend.

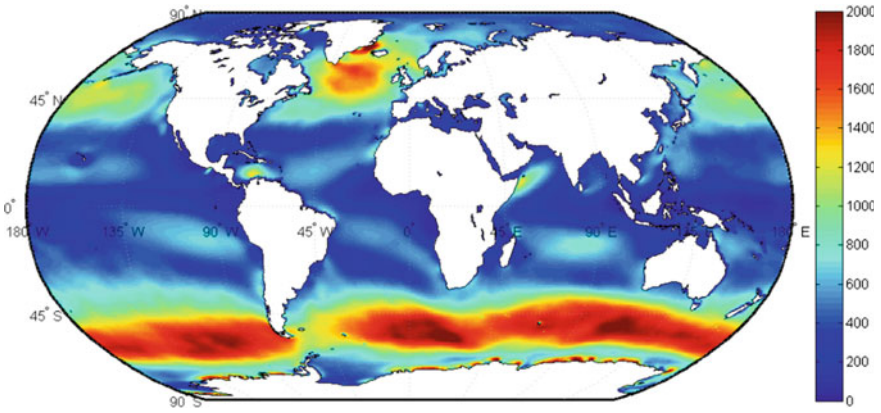

Fig. 16 MERRA Mean annual wind power density (W/m^2) for 2014 at 80 m (extrapolated from 10 m using power law and exponent = 0.14)

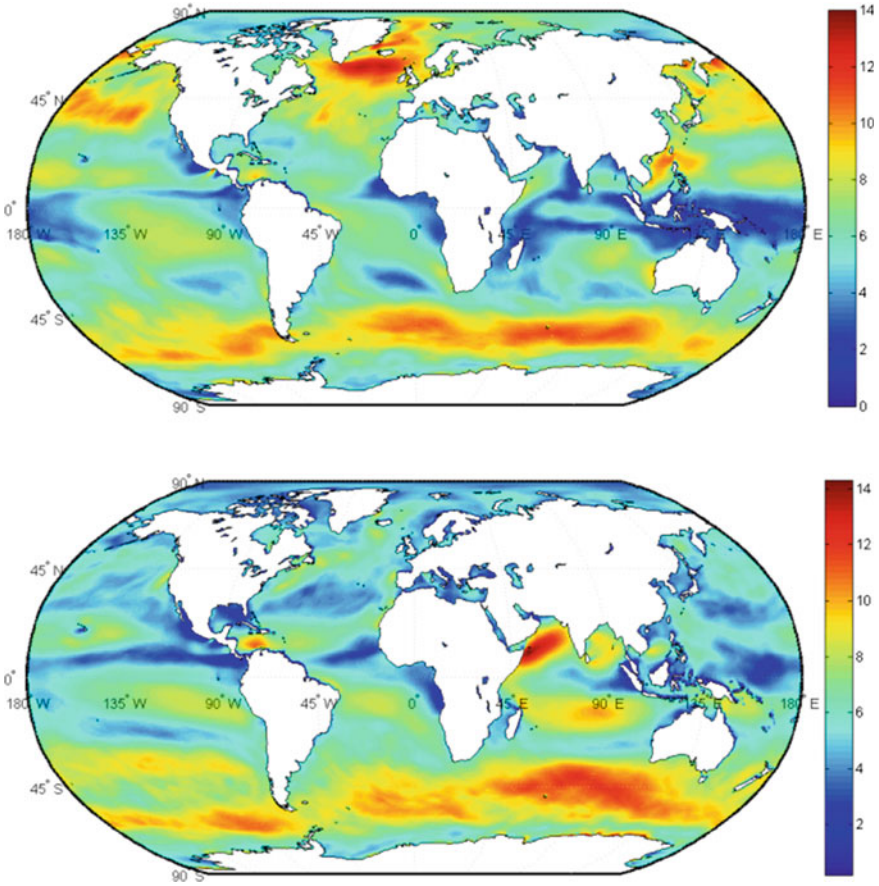

Fig. 17 MERRA Mean December (*top*) and July (*bottom*) surface level wind speed (2014)

The Atlantic coast of Europe has a very strong wind resource, and generally, the wind speeds are higher along the northern areas of this coast, compared to those in the south. The winter climate is also strongly influenced by the North Atlantic Oscillation, a phenomenon which refers to the presence of a low pressure centre over Iceland, and a high pressure located around the Azores, to the west of Portugal. Since winds in the northern hemisphere will always blow with the pressure centre to the left of the wind vector, this leads to a strong tendency for dominant west-south-westerly winds to blow in from the Atlantic. A weather classification system known as *Grosswetterlagen* categorises the circulation patterns over Europe into 29 distinct patterns (Hess and Brezowsky 1952) with the most frequently occurring types being *anti-cyclonic westerly*, *cyclonic westerly* and *maritime westerly* (James 2007), all three of which are dominated by the Icelandic low/Azores high.

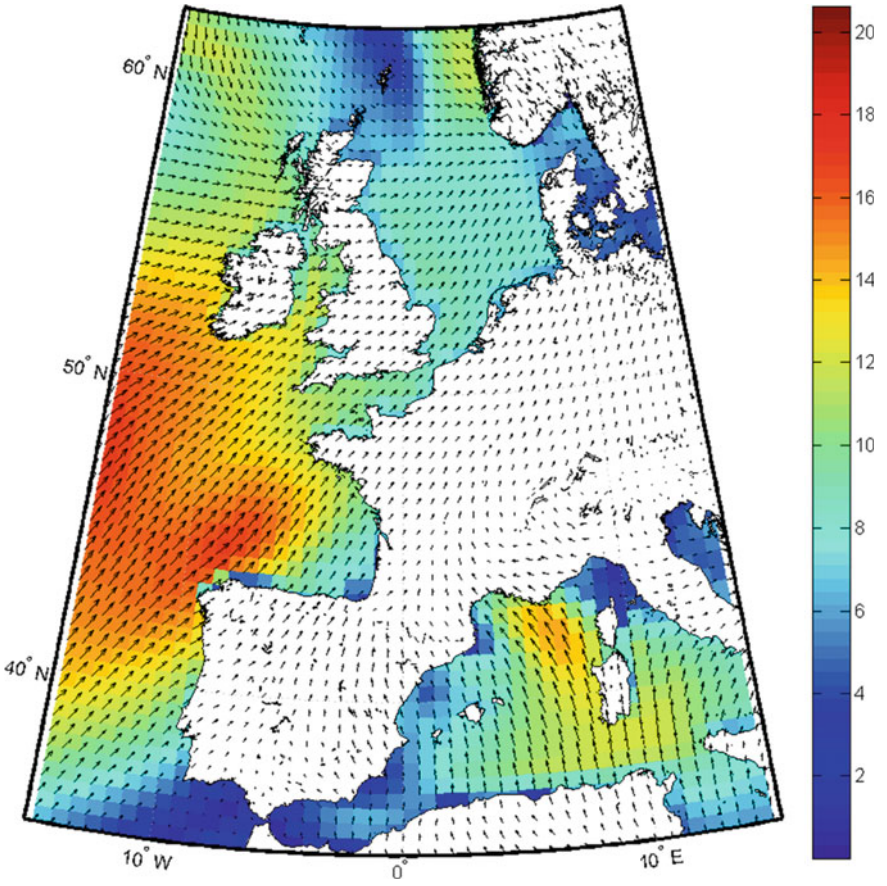

Fig. 18 Daily 10 m wind speed and vectors for January 5th 2014 over Europe

A plot of daily mean wind speed and vectors for a stormy day in January 2014 (Fig. 18) reflects the pressure pattern shown in Kendon and McCarthy (2015), with low pressure centres over the north west of Europe and also around the Mediterranean Sea area. The winds were very strong, with the daily mean reaching 15 m/s along the south-west coast of Ireland and the north-west of Spain. There are also very high winds shown in the northern Mediterranean Sea, to the south of France. It can be seen that the North Sea is somewhat more sheltered, whilst still experiencing relatively strong winds.

As an indicator of the pattern of extreme winds over the whole of 2014, the map of the 95 % percentile daily mean wind speed in 2014 from MERRA is shown in Fig. 19. This shows, as might be expected, the most severe conditions occurring along the north-western Atlantic coasts of the British Isles and Norway. Values of above 10 m/s are seen along all western shores north of Portugal and also throughout the North Sea, and in part of the Mediterranean Sea.

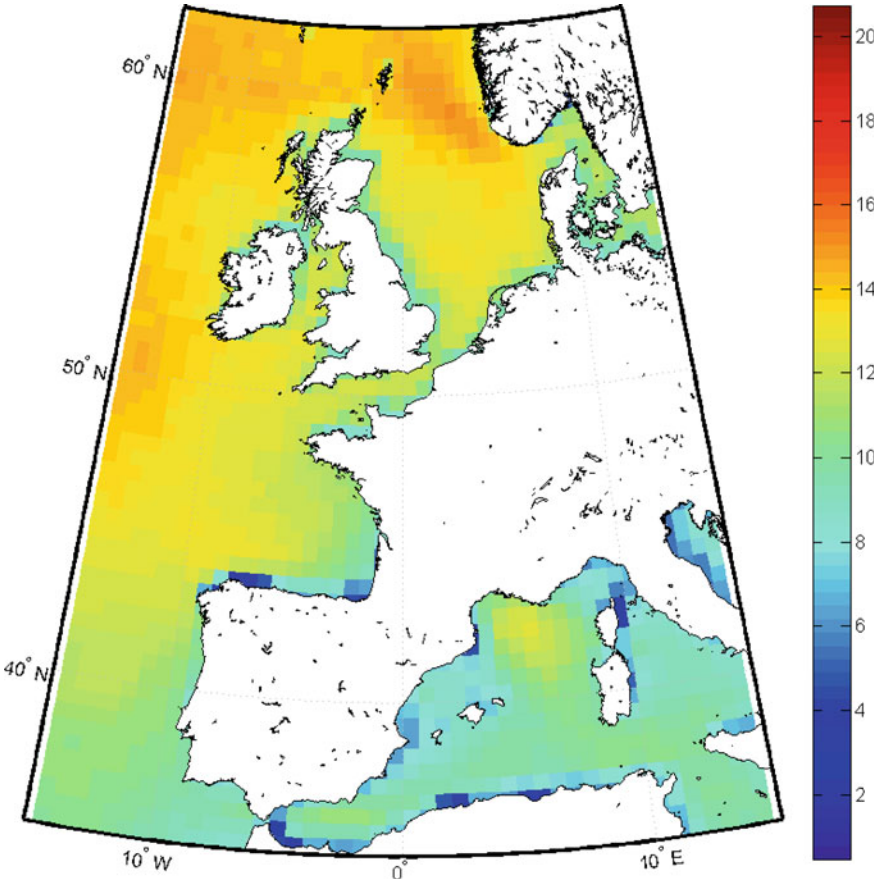

Fig. 19 95th percentile of daily average 10 m wind speed from MERRA in 2014

Both Figs. 18 and 19 demonstrate that there is an issue with the resolution of the coastline in the MERRA model, which is particularly evident along the north coast of Spain. The low values given by the model here are perhaps not as would be reflected by measurements in this area but due to the model resolution, it cannot always capture the true conditions. This should be taken into account when analysing coastal wind speeds from any model.

1.4 Discussion

Over the last 20–30 years, since the onshore wind energy industry became established, it has seen an enormous amount of rapid development. The experience that has been obtained has led to significant improvements in efficiency, reliability and

design. It is now important to be able to use this knowledge to accelerate the development of offshore wind. When considering the offshore wind energy resource, it is important to bear in mind the differences compared to the conditions experienced onshore, and how this will impact on a site in terms of power production and reliable design. The mean wind speeds experienced far offshore are typically higher than those found onshore, and are in general found to show less variability in time and space. This would indicate that in terms of power production, offshore sites are more favourable. It is important to consider, however, that some of the assumptions used—for example, to calculate vertical wind shear—are perhaps not automatically transferrable from on-to offshore. In particular, throughout this section, reference has been made to the fact that conditions in coastal regions often show significant deviation from expected patterns, and are particularly difficult to model. In this case, measurement campaigns are critical to understanding the resource, exploiting it optimally and dealing with the difficulties. Additionally, as computing power becomes cheaper and more accessible, the ability to incorporate new knowledge and model these zones effectively becomes easier, providing a more complete picture of the conditions.

2 Wave Climate

Pauline Laporte Weywada

The knowledge of waves has been a topic of research for many decades, as it defines in a large measure the design and operational safety of offshore structures such as oil platforms. Estimating the environmental loads acting on a FOWT and its support structure therefore requires the quantification of the local wave climate. The accurate characterisation of the wave resource will establish and inform the relevant environmental conditions for the design of the support structure at the proposed location.

2.1 Origins of the Resource

Classification and Origin of Ocean Waves

Ocean wave is a generic term that gathers very different types of waves. Various studies have aimed at providing a classification of ocean waves, one of the first being proposed by Munk (1950). The classification is based on the energy source that creates the wave, and their period or wave length. Table 2 summarises the ocean waves categories defined by Munk.

The category of ocean waves proposed by Munk with the largest period is the *trans-tidal* waves. These are generated by low frequency fluctuations in the Earth's

Table 2 Tentative classification of ocean waves according to wave period (based on Munk 1950)

Classification	Period	Source
Trans-tidal waves	24 h and up	Storms, sun and moon
Ordinary tides	12–24 h	Sun and moon
Long-period waves	From 5 min to 12 h	Storm and earthquakes
Infra-gravity waves	From 30 s to 5 min	Wind
Ordinary gravity waves	From 1 to 30 s	
Ultra-gravity waves	From 0.1 to 1 s	
Capillary waves	Less than 0.1 s	

crust and atmosphere. The gravitational pull of the sun and moon on the earth also causes waves, with a period of between 12 and 24 h. These waves are *tides*. The next type of waves in the ocean wave classification are *long-period waves* generated by severe storms, with low atmospheric pressure and the high wind speed. Other hazardous waves can also be caused by underwater disturbances that displace large amounts of water quickly such as earthquakes, landslides, or volcanic eruptions. These very long waves are called *tsunamis*. The shortest period waves are called *capillary waves*, generated by wind but dominated by surface tension.

However, the most common association with the term *ocean waves*, and the focus of this section, are surface waves with periods between 0.1 and 30 s. These are dominated by gravity and caused by wind blowing along the air-water interface, creating a disturbance that steadily builds as wind continues to blow and the wave crest rises. These wind-driven waves can be separated in two sub-categories: the irregular and short crested *wind sea*, when they are generated by local wind; and the more regular and long-crested *swell*, when the wave system leaves its generation area.

Sea State and Wave Spectrum

The wind-driven generation of waves is a highly chaotic phenomenon that cannot be described by a single time record of the sea surface. Instead, for resource characterisation the use of a frequency domain representation of the sea surface is largely adopted, in which the wave system is represented as the sum of a large number of elementary component wave trains with different frequencies and directions and random phases. This directional wave spectrum describes the complex phenomenon of wind-generated ocean waves in terms of contributions from waves propagating in different directions with different wavelengths. Its purpose is to describe the sea surface as a stochastic process, i.e. to characterise all possible time records that could have been made under the conditions of the actual observation.

The directional wave spectrum is a fundamental parameter of wave modelling that quantifies the relationship between energy content and directional distribution. The forces acting on offshore structures and their response to waves depend on the characterisation of the directional spectrum.

The basic concept of the wave spectrum flows from the decomposition of any record of surface elevation, $\eta(x, y, t)$, as the sum of a large number of harmonic wave components, i.e. as a Fourier series:

$$\eta(x, y, t) = \sum_{p=1}^{P} a_p \cos\left(2\pi t f_p - \mathrm{k}_p x \cos\theta_p - \mathrm{k}_p y \sin\theta_p + \alpha_p\right) \tag{13}$$

where the amplitude a_p, wave number $\mathrm{k_p}$, wave direction θ_p and direction of wave propagation α_p describe the wave components. Two basic approaches, following stochastic and deterministic principles, are possible to describe the wave field as presented in Benoit et al. (1997).

Stochastic methods are based on the random phase assumption, and the wave field can then be described in a continuous way as:

$$\eta(x, y, t) = \iint \sqrt{2S(f, \theta) df d\theta} \cos(2\pi t f - \mathrm{k} x \cos\theta - \mathrm{k} y \sin\theta + \alpha) \tag{14}$$

where the variance density spectrum $S(f, \theta)$ and the wave amplitude a are linked following linear assumptions:

$$S(f, \theta) = \lim_{\Delta f \to 0} \lim_{\Delta\theta \to 0} \frac{1}{\Delta\theta \Delta f} \mathrm{E}\left(\frac{1}{2}\mathrm{a}^2\right) \tag{15}$$

As the phase function is randomly distributed, the wave components are independent from each other and these methods are typically unsuited for situations where phase-locking may occur (e.g. close to a reflective structure). In such occasions, the deterministic approach is preferred.

The following conventional decomposition of the directional spectrum is often used:

$$S(f, \theta) = E(f) D(\theta, f) \tag{16}$$

The one-dimensional frequency spectrum $E(f)$, which does not contain any directional information, can be obtained from this frequency-direction spectrum by integration over all directions:

$$E(f) = \int_0^{2\pi} S(f, \theta) d\theta \tag{17}$$

The direction distribution, or directional spreading function $D(\theta, f)$ is defined such that:

Table 3 Definition of the key spectral parameters

Spectral nomenclature	Definition	Description
H_{m0}	$4\sqrt{m_0}$	Significant wave height (H_s)
T_{m-10}	m_{-1}/m_0	Energy period (T_e)
T_{m01}	m_0/m_1	Mean period (T_m)
T_{m02}	$\sqrt{m_0/m_2}$	Zero-upcrossing period (T_z)

$$\int_0^{2\pi} D(\theta,f)d\theta = 1 D(\theta,f) \geq 0, \quad [0,2\pi] \tag{18}$$

The latter expresses that the directional spreading function is a non-negative function, whilst the former is a direct consequence of the definition of the frequency variance spectrum.

The main statistical characteristics of wind waves that can be extracted from the frequency spectrum $E(f)$ are described in Table 3, expressed in terms of the *nth*-order moments of that spectrum:

$$m_n = \int_0^{\infty} f^n E(f)df \quad \text{for } n \in \mathbb{Z} \tag{19}$$

Typically, a sea state is characterised by the significant wave height, a spectral period such as the zero-upcrossing period, main direction and the shape of the spectrum. Following Goda (2000), the zero-upcrossing period relates to the mean period between consecutive crests, where the surface profile crosses the zero line upwards in a time-series surface elevation plot (relative to the mean water level). Depending on its nature, the shape of the spectrum can vary significantly, and several models exist to fit the conditions, as described at the end of this sub-section.

The one- or two-dimensional spectrum is acquired using in situ or remote-sensing measurements of the sea-surface, or using numerical wave models based on wind, tide and seabed topography information. These techniques are detailed further in Sects. 2.2 and 2.3.

Wave Propagation and Transformation of the Wave Resource

In the near-shore region, several factors are involved in the wave physics and interact to various extents with the waves changing their characteristics, in terms of the total wave energy as well as directional spectrum distribution of that energy. These are complex physical processes that need to be taken into account when considering wave propagation in shallow water. They can be categorised as wave interaction processes with the atmosphere, the seabed, the current or with other

waves, as presented below. A general description of each of these wave transformation process is given by Sarpkaya and Isaacson (1981).

As well as being a driving phenomenon in the wave generation, the wave-atmosphere interaction also takes part in energy dissipation processes such as white capping or wave propagation against the wind. The former is also known as wave breaking, and is due to an excessive wave steepness during wave generation and propagation. Breaking waves play a major role in the engineering design of offshore structure because the effect can be considerable (Young 1999): the accelerations that are involved in those situations are often large and potentially damaging if they impact a structure. The average wave steepness for an irregular sea state is defined as:

$$S_x = \frac{2\pi}{g}\frac{H_s}{T_x^2} \tag{20}$$

where S_x is the wave steepness relating to the period parameter T_x (typically, zero-crossing period T_z, peak period T_p or mean wave period T_m). Unless site-specific information is available, the limiting steepness S_z can be taken as 1/10 for $T_z < 6s$, 1/15 for $T_z > 12s$ and interpolated linearly between the two (DNV-RP-C205 2010).

Energy dissipation processes also occur with wave-bottom interaction such as bottom friction, essentially a transfer of energy and momentum from the orbital motion of the water particles just above the seabed in the turbulent boundary layer. Bottom friction causes wave height reduction as the water depth becomes more and more shallow and is of special importance over large areas with shallow water. Wave breaking can also occur with wave-bottom interaction, when the wave height becomes greater than a certain fraction of the water depth. Other wave-bottom interaction effects are depth-induced refraction which, at small depths, modifies the directions of the wave and then implies an energy transfer over the propagation directions, and shoaling where the wave height variation process as the water depth decreases, due to the reduced wavelength and variation of energy propagation velocity. Diffraction by a coastal structure (breakwater, pier, etc.) result in an energy transfer towards the shadow areas beyond the obstacles blocking the wave propagation.

Wave-current interaction can dissipate energy through wave blocking due to strong opposing currents, or affect the wave propagation process through current-induced refraction, which causes a deviation of the wave and an energy transfer over the propagation directions, or interactions with unsteady currents, inducing frequency transfers (e.g. as regards tidal seas).

Finally, non-linear wave-to-wave interaction can occur at great depths (mostly resonant quadruplet interactions) and small depths (mostly triad interactions), these interactions are further described in Hasselmann (1962, 1963).

Wave generation, interactions and dissipation processes need to be accounted for when considering the propagation of waves to a specific prediction point in numerical wave models. The first generation model did not consider nonlinear wave interactions. Second generation models, available by the early 1980s, parameterised these

interactions. Third generation models, further presented in Sect. 2.3, explicitly represent all the physics relevant for the development of the sea state in two dimensions.

Short Term Wave Conditions

A typical sea state may consist of several spectral components: one generated locally by local winds (wind-driven component), plus one or more swell components. These various components, to a good approximation, behave in a simple additive fashion, as regards both water movements and energy flows.

During the last decades, several wave spectrum models have been proposed to characterise short term stationary irregular sea states. Today the Pierson and Moskowitz (1964) model is the most generally accepted to describe fully-developed wind-driven wave systems. These situations occur when stable conditions have prevailed for a long period, in a long enough fetch. In younger seas or for shorter fetches, the JONSWAP experiment showed that the wave system may not have the time to fully develop (Hasselmann et al. 1973). This typically leads to a higher peak at a higher peak frequency. As the sea state develops, the nonlinear wave-to-wave interactions move the peak toward lower frequencies and flatten it, converging to the Pierson-Moskowitz model. The model used since to describe developing sea states is generally known as the JONSWAP spectrum.

After the wind ceases to provide input to the waves, they propagate freely as swell, travelling away from the storm area. Long waves travel faster than the short ones, and the swell system progressively loses its high frequency components, becoming more peaked and less broad banded.

When the peak frequencies are well separated, the spectrum has a double (or more) peak. Several double-peak spectra models have been proposed to describe such mix sea states. Strekalov et al. (1972) suggested the combination of one high frequency spectrum describing the wind-driven wave system and a Gaussian shaped model describing the swell. Ochi and Hubble (1976) combined a JONSWAP and a Pierson Moskowitz spectra. Guedes Soares (1984) and then Torsethaugen (1993) adopted two JONSWAP spectra using respectively four and seven parameters.

When considering individual waves, the short term distribution of individual wave heights can be modelled using a 2-parameter Weibull distribution, based on Forristal (1978).

$$F_H(h) = 1 - \exp\left(-2.263\left(\frac{h}{h_s}\right)^{2.126}\right) \tag{21}$$

where h is the wave height and h_s the significant wave height.

Intermediate Time Scales

Seasonal Variability

Aside from a large spatial variation in wave resource, a significant seasonal variability can also be evidenced by comparing the wave climate in winter and summer. Challenor et al. (1990) used satellite wave height measurements during the period between November 1986 to November 1987 to map the seasonal variations in the

global wave climate. The largest significant wave heights occurred during winter in the Southern Ocean (June–September) with only a slight reduction during the southern summer (December–March). In the North Atlantic and North Pacific the significant wave heights were lower and there was a larger variation between summer and winter.

Young (1999) presented significant wave height, peak and mean wave period and wave direction in terms of mean monthly statistics. The data set presented by Young (1999) was obtained from a combination of satellite remote sensing and model predictions covering a 10-year period. The results highlight the zonal variation in wave height, with more extreme conditions occurring at high latitudes. The important role played by the intense wave generation systems of the Southern Ocean was also evidenced, where swell generated from storms in the Southern Ocean penetrates throughout the Indian, South Pacific and South Atlantic Oceans. During the Southern Hemisphere winter, this swell propagates into the North Pacific.

At a local scale, seasonality effects are also typically studied as part of a site assessment. An example can be found in the resource assessment for the WaveHub site, Cornwall, as part of the Marine Energy in Far Peripheral and Island Communities (MERIFIC) project, presented in Smith and Maisondieu (2014). The seasonal power variation, with the mean power calculated for spring (March–May), summer (June–August), autumn (September–November) and winter (December–February) months are presented in Fig. 20. The monthly variation in T_{m-10} is

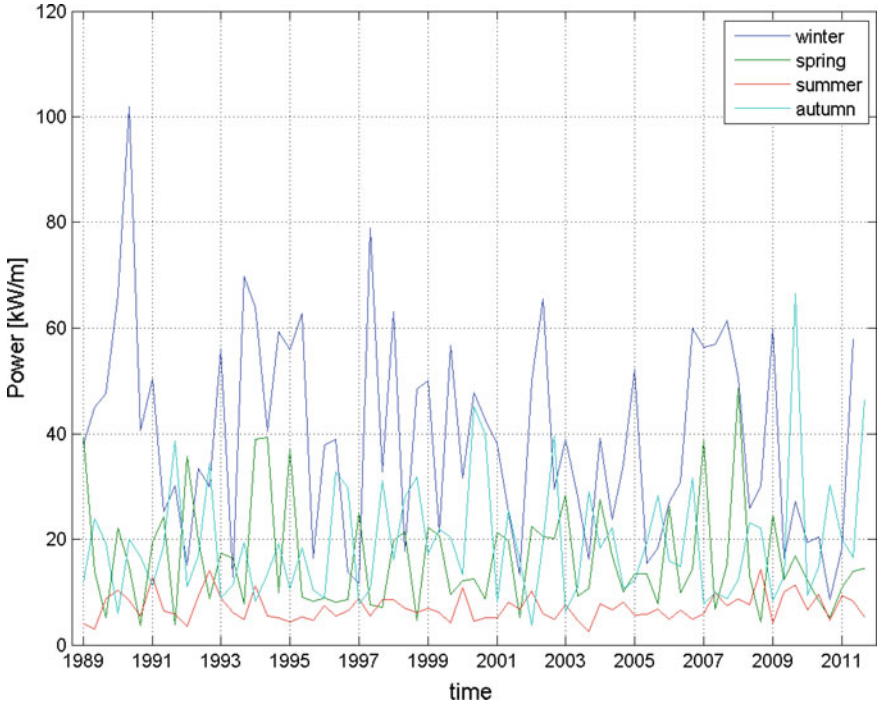

Fig. 20 Seasonal variation of power at Wave Hub (Smith and Maisondieu 2014)

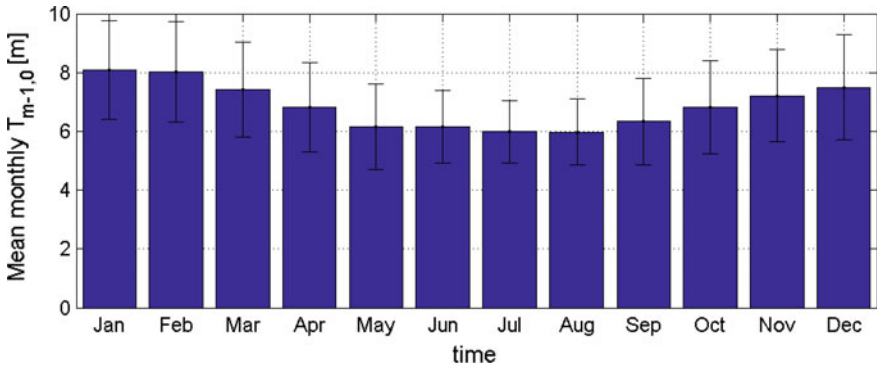

Fig. 21 Monthly variation of T_{m-10} at Wave Hub, with bars showing the standard deviation in the data (Smith and Maisondieu 2014)

shown in Fig. 21. The variation in power levels over each year is substantial. Averaged over the entire dataset, it can be seen that the winter months are the most energetic.

Marine Operations

For certain design situations involving marine operations in the order of days or of weeks, an important aspect of the wave climate that must be considered involves the expected occurrence of weather windows that allow for operations such as transport, deployment, recovery and maintenance. The objective is to avoid delays in critical marine operations due to significant wave heights exceeding prescribed operational levels (limits), leading to a possible increase in the duration of the operations and/or increased damage to the FOWTs. In such cases, the probability of occurrence of sea states in which H_s, is at, or below, a specified threshold value, for at least a specified number of hours, combined with the wait time for a number of weather windows specified by a H_s threshold and minimum window length is of interest to the project developer. An example of characteristic durations of operation limited by a given significant wave height for a given number of hours, along with the expected *mean* duration, and 10, 50 and 90 percentiles (*P10*, *P50* and *P90* respectively) is given in Fig. 22, taken from a Statoil study presenting a metocean design basis for a proposed FOWT installation site in Scotland (Mathiesen et al. 2014).

Long Term Wave Conditions—Extremes

The assessment of extreme wave conditions is essential to the design of floating support structures. For design considerations, interest is often on the most likely maxima or on the extreme values that occur within a very long period of time.

The long-term variation of the wave climate can be described in terms of generic distributions or in terms of scatter diagrams for governing sea state parameters such as H_s, T_z or θ. A scatter diagram provides the frequency of occurrence of a given parameter pair (e.g. H_s, T_{m02} as shown in Fig. 23). Both marginal distributions and

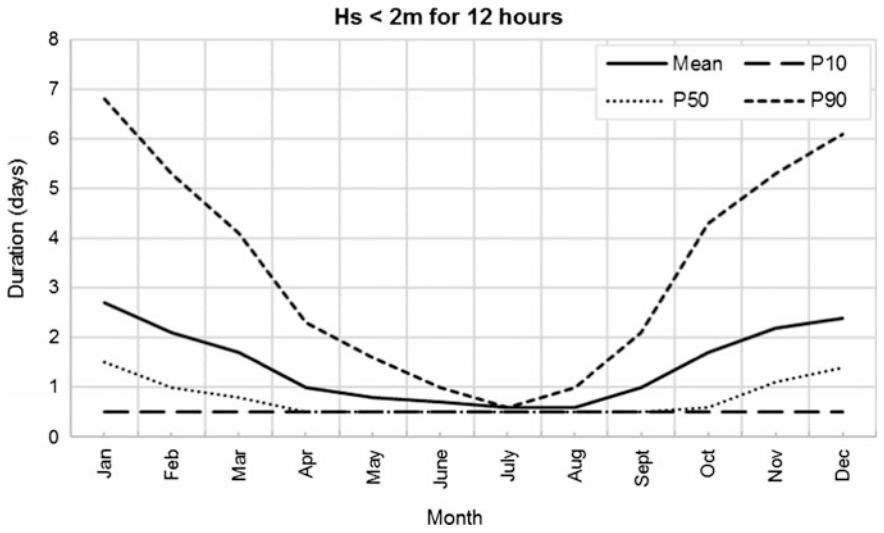

Fig. 22 Characteristic durations, including waiting time, in order to perform operations limited by a significant wave height of 2 m for 12 h (figure based on data presented in Mathiesen et al. 2014)

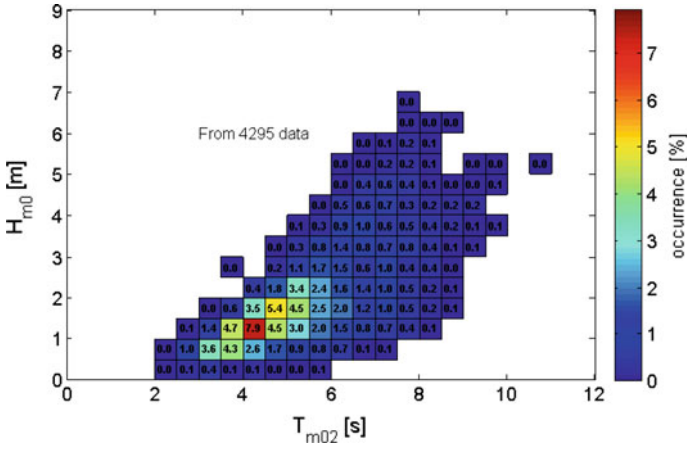

Fig. 23 Annual $H_{m0} - T_{m02}$ scatter plot for the Wave Hub region using data from November 2009 to October 2010 from a combination of ADP and wave buoy records (Smith and Maisondieu 2014)

joint environmental models can be applied to describe the wave climate. The generic models are generally established by fitting distributions to measured wave data from the site of interest.

In cases where the weather is relatively calm most of the time, and there are few very intense events, an event based approach is used for the analysis of the wave

data, where observations over some threshold level are used (e.g. Peak Over Threshold, POT, method). In an event based model like POT, the results may be sensitive to the adopted threshold level. A lower threshold decreases statistical uncertainty (by allowing more peaks over the threshold) but may reduce the accuracy by including data points that do not belong in the tail of the distribution. A suitable threshold will be associated with stable estimates beyond its value, and exponential distribution or a two-parameter Weibull distribution can then be fit with more confidence to the remaining data points.

The annual extremes of an environmental variable, for example the significant wave height or maximum individual wave height, can be assumed to follow a Gumbel distribution;

$$F(H_s) = \exp\left(-\exp\left(-\frac{H_s - U}{A}\right)\right) \tag{22}$$

where A and U are distribution parameters related to the standard deviation and the mean of the Gumbel distribution.

The significant wave height with return period T_R in units of years is then given by:

$$H_{s,T_R} = F^{-1}\left(1 - \frac{1}{nT_R}\right) \tag{23}$$

where $\left(1 - \frac{1}{nT_R}\right)$, is the quantile of the distribution of significant wave heights, with n the number of sea states per year. To accompany the H_{s,T_R} significant wave height and complete the definition of the T_R year design sea state, the T_p or T_z values are typically varied within a period band about the mean or median period.

For reliability analysis, joint environmental models can be used. A common approach for establishing a joint environmental model is the Conditional Modelling Approach (CMA) (e.g. Bitner-Gregersen and Haver 1991), where a joint density function is defined in terms of a marginal distribution and a series of conditional density functions. For example, for a joint distribution of significant wave height and period:

$$f_{H_s T_z}(h,t) = f_{H_s}(h) \cdot f_{T_z|H_s}(t|h) \tag{24}$$

Often, the probability density function for the significant wave height is modelled by a 3-parameter Weibull distribution and the zero-crossing wave period conditional on H_s is modelled by a lognormal distribution. For a joint distribution of significant wave height and wind speed, Bitner-Gregersen and Haver (1989, 1991) use a 2-parameter Weibull distribution which can be applied for the mean wind speed U conditional on H_s.

Other approaches for establishing a joint environmental model exist, such as the Maximum Likelihood Model (MLM) (Prince-Wright 1995), or the Nataf model (Der-Kiureghian and Liu 1986).

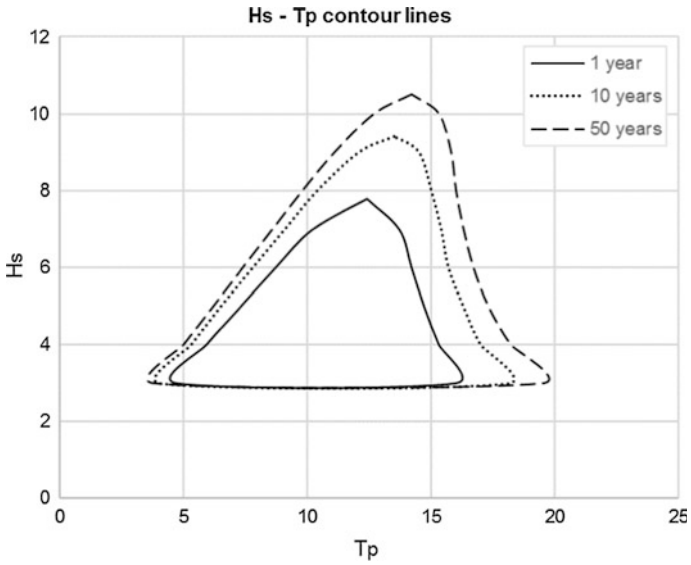

Fig. 24 $H_s - T_p$ probability contour lines for return periods of 1, 10 and 50 years, for omni-directional waves at a specific site (figure based on data presented in Mathiesen et al. 2014)

The environmental contours can then be defined in the environmental space from the joint environmental model of sea state variables (e.g. H_s, T_p, as shown in Fig. 24) (Winterstein et al.1993). A common method to define these contours is to estimate the extreme value for the governing variable for the prescribed return period, e.g. H_s, and associated values for other variables, e.g. T_z. The contour line is then estimated from the joint model or scatter diagram as the contour of constant probability density going through the above mentioned parameter combination.

Following Battjes (1978), the maximum individual wave height in a random sea state can be expressed as:

$$F(H_s) = \frac{1}{\overline{v_0^+}} \iint_0^\infty v_0^+ \left(h_s, t_p\right) F_{H|H_s T_p}\left(h|h_s, t_p\right) f_{H_s T_p}\left(h_s, t_p\right) dh_s dt_p \tag{25}$$

where $v_0^+\left(h_s, t_p\right)$ is the expected zero-up-crossing wave frequency for a given sea state and $\overline{v_0^+}$ is the long term average zero-up-crossing wave frequency given by:

$$\overline{v_0^+} = \int \int_0^\infty v_0^+ \left(h_s, t_p\right) f_{H_s T_p}\left(h_s, t_p\right) dh_s dt_p. \tag{26}$$

The individual wave height with return period T_R (in years) then follows from:

$$1 - F(H_{T_R}) = \frac{1}{T_R \cdot 365 \cdot 24 \cdot 3600 \cdot \overline{v_0^+}} \tag{27}$$

The extreme sea state characterisation can be made based on measurements of the sea-surface, or using numerical wave models based on wind, tide and seabed topography information. These techniques, and their limitations, are detailed further in the following sections.

2.2 Measuring the Resource

Measurement techniques can be divided in two categories: in situ techniques, where the instrument is deployed in the water, and remote-sensing techniques, where the instrument is deployed at some distance above the water.

When making measurements to determine the wave resource, it is important to have a clear understanding of how representative the measurement is of the area in which the measuring instrument is situated. This depends on the exposure of the measurement site to the prevailing waves in terms of sheltering, and of the bathymetry of the area surrounding the wave measurement site.

In Situ Techniques

Wave Buoys

The most common in situ instruments are wave buoys. Such instruments have been used for measuring waves since the early 1960s. The buoy follows closely the motion of the water particles by floating at the surface, and measures its vertical acceleration with an on-board accelerometer, stabilised on a gravity platform for artificial horizon reference. The sea surface elevation is obtained by integrating twice the vertical acceleration (the small horizontal motion is ignored). Three of the main manufacturers of wave measurement buoys are OCEANOR, Datawell and TRIAXYS. Each produces a range of directional and non-directional buoys for different applications, examples of some available wave buoys are illustrated in Fig. 25.

In order to measure the direction of the wave, the buoy sensor can be refined to also measure its inclination with the horizontal. Two methods are mostly used. The first type calculates the slope of the sea surface from the pitch and roll motions of the buoy. The mean direction is determined from the tilt, measured with inclinometers, and the direction to the geographic North. Such buoys are usually relatively flat, like the WAVEC buoy (Wave-VECtor, a Datawell buoy). The second type uses the sway and surge motions of the buoy to determine its tilt. The Directional WaveRider buoy from Datawell uses the Earth's magnetic field to measure its tilt, and a study conducted by Barstow and Kollstad (1991) showed that

Fig. 25 Seawatch Wavescan buoy (www.oceanor.com) (*left*), Datawell Waverider buoy (http://www.datawell.nl) (*centre*), Seawatch Midi 185 buoy (www.oceanor.com) (*right*)

this leads to reliable data when compared with a Wavescan buoy. Some other wave buoys, like the GPS-WaveRider, use a global positioning system (GPS).

When deploying wave buoys, a compromise must be considered between station keeping and minimal impedance to the buoy motion requirements. Site specific water depth, current and wave climate must be taken into account when designing the moorings that will keep the buoy on station. Aside from mooring compliance and limitation, steep waves also bring bias in the wave buoy motion, with the natural tendency of the buoy to bypass the crest, leading to smaller estimates of the wave height.

The time series data recorded by wave buoys is processed into auto- and cross-spectra, from which the variance density spectrum and the directional distribution can be obtained. It should be noted that integrating acceleration data to obtain displacements is difficult as very low frequencies or offsets are present. Typically, the lower frequencies are amplified with the noise superimposed. A difficulty arises when considering that the use of a high pass filter has the effect of also filtering the second order non-linear part of the waves, and leading to a bias of the measured heights of the wave crests.

Data recorded and post processed by the buoy can be stored on-board, or regularly transmitted to the shore. Data transmission, often used to avoid the weather-window limitation (especially during winter months), can be achieved by standard communication systems such as radio (HF, VHF, GPRS systems) or satellite (ARGOS, ORBCOMM etc.). However, data transmission, especially via radio, can be compromised in for example large waves events. When storing data on-board, manual downloads on a periodic basis, depending on the data storing capacity, will be required. Access to the buoy will also be required typically once to twice a year for battery replacement and check/re-calibration of instrumentation.

Acoustic Doppler Profilers (ADPs)

Although initially developed for current measurements, ADPs have been further developed to enable wave spectrum estimates. Three different technics can be used for sea surface wave measurements.

The first technique leads to a directional spectrum, using the cross-spectra obtained from the along-beam component of the wave orbital velocity. The cross-spectra gives the phase difference between the different beams, which then gives the wave direction and wavelength.

Two other techniques enable the calculation of the omni-directional spectrum. Surface tracking is the echo location, using the ADP beam(s), of the range to the surface. The signal of the inverted echo-sounder is reflected off the water surface, which produces a time series of sea surface elevation. The pressure sensor technique also measures the sea surface elevation via dynamic pressure measurements, but is very sensitive to wave number and is therefore mostly used for redundancy and data quality check.

Two of the most commonly used ADPs for wave measurement are Teledyne RD Instruments' Workhorse Waves Array and Nortek's AWAC with Acoustic Surface Tracking (AST). Both use the three different techniques introduced above to describe the waves.

ADPs can be mounted on the seabed or on a sub-surface buoy. The former is more secured and less vulnerable to damage, but the accuracy at high frequency can potentially be decreased by larger water depths. A compromise must then be considered between accuracy and vulnerability. Furthermore, a bottom mounted ADP can be subject to burying by the bottom soil and compromise the data acquisition; this additional risk should also be taken into account when considering ADP deployment, depending on the bottom soil at the measurement site.

Data recorded and post processed by the ADP can be stored on-board, or regularly transmitted to the shore. Data transmission, often used to avoid the weather-window limitation (especially during winter months), can be achieved by standard communication systems such as radio (HF, VHF, GPRS systems) or satellite (ARGOS, ORBCOMM etc.). However, similar to a wave buoy, data transmission can be compromised in large waves events. When storing data on-board, manual downloads on a periodic basis, depending on the data storing capacity of the instrument, will be required. On top of manual downloads, access to the ADP will also be required typically once to twice a year for battery replacement and check/re-calibration of instrumentation.

Remote-Sensing Techniques

HF and X-Band Radars

HF radar is a shore-based remote sensing system using radio waves in the 3–30 MHz region to measure directional wave spectra and surface currents. It requires two shoreline transmitter/receiver stations to be set up so that the *look* directions are approximately at right angles, with overlapping transmission region.

Subject to a number of limitations, the full directional spectrum can be measured on a grid defined by the intersection of the radar beams with a spatial resolution typically between 300 m at best, for short-range systems, and 5 km. The temporal resolution is typically a maximum of 10-min. The radar operating range, typically between 10 and 100 km, defines the range of H_s that can be observed and the highest wave frequency measurable.

On most occasions the spectrum can be measured accurately using remote sensing systems, but there are occasions when this is not so. This is because the data interpretation (inversion) technique is quite sensitive to imperfections in the radar data. Of the directional parameters, mean direction is reasonably reliable but directional spread may not be very accurate. Comparisons of wave power estimates suggest that differences between buoy and radar measurements are mostly comparable with the (joint) sampling errors associated with the two methods.

Based on the phenomenon of Bragg scattering of the transmitted waves by ocean waves of exactly half their frequency, the Doppler spectrum of the radio backscattered waves is observed. The frequencies of the two discrete peaks of the Doppler spectrum can be used to determine the surface currents. The directional spectrum of the ocean waves is then obtained by inversing techniques.

The main advantages of HF radar compared to in situ measurements such as wave buoys or ADP systems are two-folds: the spatial coverage that a HF radar system is up to 40 by 40 km, which would be very difficult (e.g. in terms of maintenance and costs) to obtain with in situ measurement methods; the easy access to the land-based instrumentation also provides a significant advantage over other in situ or satellite measurements.

The X-band radar is based on a similar technique to that of the HF radar, but uses shorter electromagnetic waves of about three centimetres wavelength. Such short wavelength interacts with surface ripples, which makes the X-band radar valuable for wave measurements in sites with light wind generating ripples on sea surface, where other techniques are unlikely to be successful.

The technique allows high-resolution directional spectra to be derived from radar images over ranges of a few kilometres. The wave information obtained is the average over an area of the order of one half kilometre square, rather than a point measurement.

Satellite Measurements

Satellite-based wave measurement differs significantly from the previous systems discussed due to the extensive coverage available. However, this type of measurement is less suited to short-term, site-specific nearshore wave resource assessment. Due to the satellite's track and revolution time limiting the spatial and temporal resolutions; it is mostly used to obtain long-term datasets for the analysis of longer-term temporal variability. Satellite-borne remote sensors can be divided in two major categories: radar altimeter and synthetic aperture radar (SAR).

Radar altimeters measure the distance between the satellite and the sea surface. The orbit of the satellite is typically 1000 km (Krogstad and Barstow 1999). The distance between the satellite and the reference ellipsoid is derived by using the Doppler effect associated with signals emitted from marker points on the Earth's surface as the satellite orbits overhead. Variations in sea surface height are caused by the combined effect of the geoid and ocean circulation. Tucker and Pitt (2001) proposed a methodology to derive empirically the significant wave height from the rise time measured by the radar. To eliminate random variations in amplitude, results are averaged over a large number of returned pulses, leading to an accuracy of more than ± 0.5 m.

SARs produce a two-dimensional (2-D) image of the sea surface. Using a 2-D Fourier transform, these images are processed to obtain a directional spectrum, with periods typically ranging from 8 to 25 s. SAR is more suited to swell observation because of the limitation in high frequency in the direction perpendicular to the track of the satellite. Typical spatial resolution for SAR images is about 25 m, for a swath of 100 km to up to 500 km wide for some satellites (e.g. RADARSAT).

Quality Control

Quality control is a necessary step in the analysis of the data received by the wave measurement device(s). The objective is to ensure the validity of the data quality, checking for flaws in the data that would lead to potentially significant errors in the resource assessment analysis and/or the determination of extreme events.

Several factors can impair the quality of the data. Faulty electronics, errors in the transmitting process, can for example generate individual spikes in the measurements, that, if large and regular, can introduce bias in the analysis. Faulty electronics can also cause high frequency noise, that potentially affects the calculation of high order spectral moments. Typically, this is solved by introducing a maximum frequency above which any integration is not performed (in general around 0.3–0.4 Hz). The integration process to transform the acceleration measurement to a displacement signal is also often subject to distortion and cause noise, in particular in the low frequency range. This low frequency noise can sometime hide a swell component.

Due to the relatively broad-band form of the wave data, where extremes cannot be automatically assumed to be faulty, the quality control of wave records is typically challenging. However, a variety of tests have been derived and are commonly used to evaluate data quality. These tests can be carried out on the original wave time series (which requires intensive processing for a large number of tests) or on the resulting frequency spectrum. For example, IOOS (2013) provides details on the main type of tests available for quality control of in situ surface wave data. The results are recorded by inserting flags in the data files where data is of low quality. Further description of the problems of wave analysis can be found in Tucker (1993) and Tucker and Pitt (2001).

Typically, the final quality of a particular wave record is determined by visual inspection of the time series or spectra. If there are outliers or suspicious trends, then the corresponding time series or spectral files and plots should be reviewed.

2.3 Resource Mapping

Although measurements of the sea state give a good representation of the wave climate at a site, it is usually too expensive to obtain long term wave climate estimates. Covering this issue, numerical wave propagation models have been developed over the last half century, which can be used in wave resource determination in the following ways:

- To provide long-term time series of wave data from which wave climate statistics can be derived. This is known as hindcasting.
- To allow calculations of wave transformation to be made in coastal areas.
- To allow operational wave forecasting for marine operations.

Since the genesis of wave generation computer simulations, several improvements have been implemented, developing the global wave models from first to third generations. However, their purpose remains the same: to simulate the growth, decay and propagation of ocean waves based on input winds over at a regional or global scale.

The early models focused on modelling wave energy growth and dissipation. Their major limitation lies in that they do not account for the nonlinear interactions between the different wave frequencies. These models are known as first generation models. The next generation of wave models, known as second generation models used parameterised approximations to model the nonlinear spectral interactions. Finally, the third generation of wave models provide a full description of the physical processes governing wave evolution.

Global Model

A number of global wave models exist today, a brief description of some of the main models used by researchers are presented below, along with wave climate studies that have been based on them.

The WAM model (WAMDI Group 1988) is a third generation wave model developed in the 1980s that integrates the basic transport describing the evolution of the wave spectrum. It calculates explicitly the effects of non-linear wave-to-wave interactions. It is routinely run at the European Centre for Medium-Range Weather Forecasts (ECMWF). More information can be found in Gunther et al. (1992) or Komen et al. (1994).

The WERATLAS project, funded by the European Union (EU) under the Joule programme, produced an atlas of annual and seasonal (yearly, Winter and Summer) wave-climate and wave-energy statistics for a set of offshore locations distributed along the European coastline (Pontes et al. 1996). Results from the WAM model were analysed for a total of 85 data points (41 in the Atlantic and 44 in the Mediterranean), using data from the period between 1987 and 1994. A wide range of wave statistical analyses, including power and T_e, are available using an interactive software package. Members of the WERATLAS project team have continued to work on the development of what has become known as WorldWaves (Barstow et al. 2003). WorldWaves is a global database of wind and wave time series data

derived from the ECMWF operational and hindcast models and are calibrated by Fugro OCEANOR against satellite data, and where available in situ buoy data to ensure that the data are as high quality as possible.

WAVEWATCH III is a wave model that was implemented in October 2008 as a replacement for the Met Office second-generation model configuration. The UK Met Office has run and maintained a suite of wave models over the past two decades to provide predictions of wave conditions, globally and around the UK. The WAVEWATCH III model provides forecast and hindcast data for a range of applications extending from predicting offshore vessel motion characteristics to forecasts of coastal overtopping.

Two 5-day forecasts with a 3-hour resolution are run per day for a global model, covering latitude from 80 S to 80 N and longitude from 180 W from 180 E with a 30 km resolution. Two operational forecasts exist for the North Atlantic European seas, covering latitudes from 25 S to 66 N and longitudes from 68 W from 42 E with a 12 km resolution: one 3-day forecast with a 1-h resolution four times a day, and another 5-day forecast with a 3-h resolution twice a day.

Typically, hindcasting requires series of wave data available for a period of at least 10-years to allow the seasonal, year-to-year and longer-term variabilities to be taken into account when deriving wave climate statistics. For this purpose, WorldWaves combines 45-year re-analysis hindcast data with operational data to provide 50-year series of wave parameter and directional spectra. The NCEP Climate Forecast System Reanalysis Reforecast (CFSRR) that uses the WAVEWATCH III model provides a 30-year homogeneous data set of hourly 0.5° spatial resolution winds.

Another use of these global models is as sources of potential wave input data at local model boundaries. Although potentially lacking the accuracy of recorded data, the use of outputs from other models as inputs for a nearshore model can often be a better option because of its spatial distribution. Outputs from other models can be treated in the same way as point measurements, and used to provide input at intervals along the model boundaries—the model will then interpolate between the input points. A second option, depending on the models being used, is nesting. Nesting involves running a larger-scale, coarser resolution model to generate boundary conditions for a finer grid, and can be repeated on decreasing scales until the required scale is attained. These local models are briefly described below.

Local Model

Local models are wave models for coastal and near-shore areas. The purpose of such model is to perform the propagation and associated transformations of the waves from offshore to nearshore, in order to investigate the detailed distribution of the wave climate. Typically, but not always, local models may use the output from a global model for their offshore boundary conditions and calculate the wave conditions at an array of grid points in the near-shore zone. The following paragraphs describe two examples of local models, but there are of course many others.

SWAN is a refraction model developed by the Technical University of Delft (SWAN Team 2006 or SWAN Team 2009) that includes many of the important

shallow water processes as well as generation by the wind. There is thus a lot of overlap between models such as this and the global models; the difference is essentially in the long-term use of the global models by the meteorological agencies. SWAN has been designed so that it can be nested in WAM and WAVEWATCH III, allowing global outputs to feed into the near shore model.

Another local model is the MIKE-21 suite which is available on a commercial basis from the Danish Hydraulics Institute (DHI) (2015). This is a linear refraction/diffraction model based on the mild-slope equation.

These two models are third-generation spectral wave models, developed for the calculation of the propagation of random waves from deep to shallow water, accounting for the different physical processes introduced in Sect. 1.1, such as white capping, bottom friction or wave-to-wave interaction.

Model Validation and Calibration

Wave models can be fine-tuned for different sites and scenarios using a number of model-dependent parameters. The calibration of these parameters can be based on published literature or through comparison to in situ measurements. In the case of calibration using measurements, wave height and wind speed data from satellite altimeter is often used for direct validation of wave models. Wave buoys can also be used, when long-term data sets are available. Figure 26 presents an example of an analysis for a model validation, which compares observed and model data.

If the wave models can bridge gaps in measured data, the wave measurements are still essential to calibration and validation of these models. For detailed site specific assessment this will likely require a dedicated measurement programme. In situ observations obtained from buoys, ships, oil platforms and satellites can be used for this purpose. The following simple statistical parameters (Ris et al. 1999) can be calculated to validate data, with x_i and y_i the measured and model wave parameters respectively:

Bias:

$$bias = \frac{1}{N}\sum_{i=1}^{N}(x_i - y_i) \tag{28}$$

Root Mean Square Error:

$$rms_{error} = \left[\frac{1}{N}\sum_{i=1}^{N}(x_i - y_i)^2\right]^{\frac{1}{2}} \tag{29}$$

Scatter Index:

$$SI = \frac{rms_{error}}{\bar{x}} \tag{30}$$

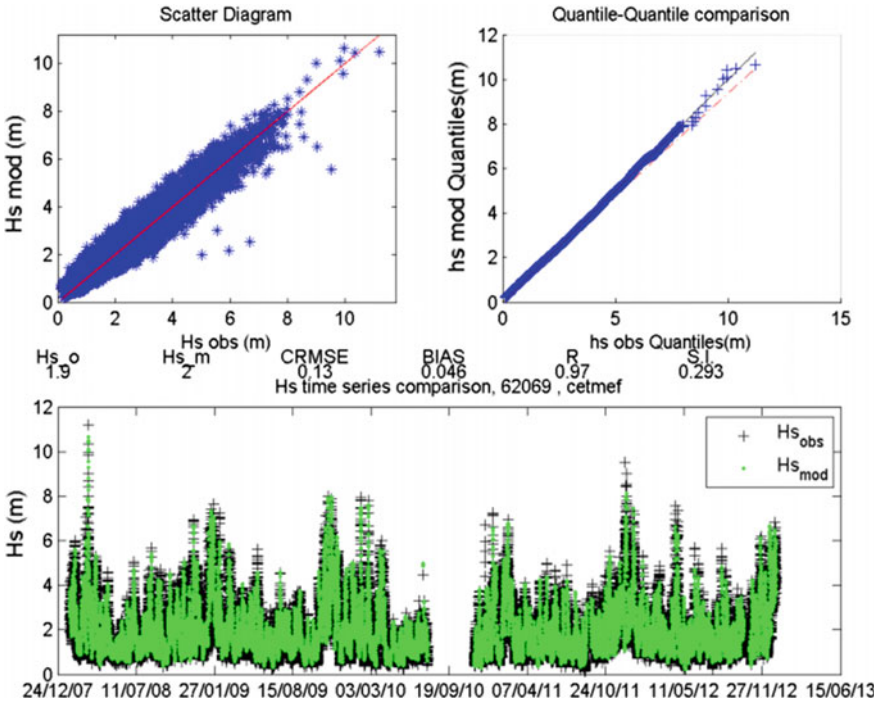

Fig. 26 Model validation—cross-comparison between buoy and numerical model output data (Smith and Maisondieu 2014)

Model Performance Index:

$$MPI = 1 - \frac{rms_{error}}{rms_{changes}} \tag{31}$$

Operational Performance Index:

$$OPI = \frac{rms_{error}}{x_i} \tag{32}$$

For example, in the WorldWaves project, satellite data from 1996 to 2002 was used to validate and subsequently calibrate the ECMWF model data. This was found to be worthwhile as there was typically a systematic bias on the raw model data. Removing that bias significantly improves the data quality, particularly in enclosed seas such as the Mediterranean Sea. Barstow et al. (2009) present the correlation coefficient between significant wave height calculated for the validation of the ECMWF wave model. A systematic underestimation of the significant wave height was found and used to calibrate the numerical model (Barstow et al. 2009). As a result, the ECMWF wave model is considered today the lead tool in its field.

2.4 Discussion

In this section a detailed account of the origin and methods to assess the wave climate were given. A knowledge of waves is essential when considering the design and operational safety of offshore structures such as floating wind turbines, and requires the quantification of the wave conditions to establish the relevant environmental conditions for the design of the structure at the proposed location.

Several methods available to estimate the directional spectrum of the waves were described. Sensors such as surface buoys, acoustic Doppler profilers or remote-sensing techniques are commonly used to characterise the sea surface. Careful consideration regarding the local bathymetry is required to ensure that the resource is representative of the target site. For a first selection of suitable areas, numerical models are commonly used and their validation against measurement, is critical.

Overall, the objective of this section has been to present the main parameters to consider to feed into the environmental load calculations and inform the design of a FOWT and its support structure, which are addressed in Chapter "Key Design Considerations".

3 Other Environmental Conditions

Mairéad Atcheson

There are several additional environmental conditions that may be considered when characterising a potential site, leading to their inclusion in a metocean design basis for a FOWT. Section 3.1 overviews the description of local current and water depth variations, including methods of measuring and modelling these variables. Other phenomena which may also be important include seismic activity and ice conditions, which are overviewed in Sects. 3.2 and 3.3 (respectively).

3.1 Currents and Sea Level

Currents

Sea currents vary in space and time, however for design purposes they are generally considered as horizontal uniform flow fields of constant velocity, varying only as a function of depth (IEC 61400-3 2009). The flow of water can be represented mathematically as a velocity vector defining the speed and direction of the current. The following components of sea current velocity should be taken into account when considering the environmental conditions at a proposed installation site:

- Sub-surface currents generated by tides, storm surges, atmospheric pressure variations, etc.,
- Wind-generated, near surface currents, and
- Near shore, wave induced surf currents running parallel to the coast.

The total current at a given location can be calculated by superimposing the vector sum of the relevant current components for the specific site to determine the variation of the current velocity with depth, referred to as the current profile. The current direction is generally described in terms of degrees measured clockwise from geographic north, and the convention is to define the direction the current is flowing in. The DNV offshore standards (DNV-OS-J101 2014) allow for the application of standard current profiles when detailed field measurements are not available to describe the current conditions. The variation in the current velocity with depth may be calculated as:

$$v(z) = v_{tide}(z) + v_{wind}(z) \tag{33}$$

where $v(z)$ is the total current velocity at level z, v_{tide} is the tidal current profile component and v_{wind} is the wind generated current component.

The tidal current profile may be characterised by a recognised power law approximation, where the variation of tidal current with depth, relative to the still water level (SWL) may be taken as:

$$v_{tide}(z) = v_{tide0}\left(\frac{h+z}{h}\right)^{1/7} \quad for\ z \leq 0 \tag{34}$$

where v_{tide0} is the tidal current at the SWL, h is the water depth from the SWL (taken as positive) and z is the vertical coordinate from the SWL (taken as positive).

The wind-generated current can be represented as a linear distribution of velocity reducing from the surface velocity to zero at a reference depth for the wind generated current below the SWL.

$$v_{wind}(z) = v_{wind0}\left(\frac{h_0+z}{h_0}\right) \quad for\ -h_o \leq z \leq 0 \tag{3.35}$$

where v_{wind0} is the wind generated current at the SWL and h_0 is the reference depth for the wind generated current [h_0 = 20 m (IEC 61400-3 2009) or 50 m (DNV-OS-J101 2014)].

The wind-generated surface current may be assumed to be aligned with the wind direction, and may be estimated from:

$$v_{wind0} = k \cdot U_0 \tag{36}$$

where U_0 is the 1-hour mean wind speed value at a height of 10 m above the SWL and k = 0.015 to 0.03 (DNV-OS-J101 2014) or 0.01 (IEC 61400-3 2009).

Where the currents at a site may vary considerably from the standard profile descriptions, site specific current profile measurements should be made.

Sea Level

The sea level at any location consists of the mean depth, defined as the distance between the seabed and an appropriate datum, and a variable component mainly attributed to astronomical tides and storm surges. Astronomical tides are generated by the gravitational pull of the moon and to a lesser extent the sun on the ocean waters of the rotating earth. Storm surges reflect changes in sea level due to meteorological forcing, including wind and atmospheric pressure effects.

The difference in height between consecutive high and low waters is described as the tidal range. A spring tide is the very highest and very lowest tide (i.e. it has the largest tidal range) which occurs twice a month (approximately every 14/15 days). Neap tides are the opposite of spring tides when the smallest tidal range is observed. The variation in water level due to the tide is described based on the lowest astronomical tide (LAT), which is the lowest level that can be predicted to occur for any combination of astronomical conditions. Similarly, the highest astronomical tide (HAT) is the highest level produced due to astronomical conditions. The best estimates of the mean water level and fluctuation (i.e. HAT, LAT and extreme water levels) are derived from site-specific measurements.

Changes in water depth due to storm surges are superimposed on the tidal variations to define the range of water levels at a site. The highest still water level (HSWL) is defined as a combination of the HAT and positive storm surge, for a given return period. Correspondingly, the lowest still water level (LSWL) is a combination of the LAT and negative storm surge, for a given return period. The relevant water levels that should be considered as a minimum are illustrated in Fig. 27. The mean sea level (MSL) is defined as the arithmetic mean of hourly observed sea levels over a period of at least 1-year, but preferably 19-years to average out the cycles of the 18.6-year nodal tidal cycle (Pugh 1996).

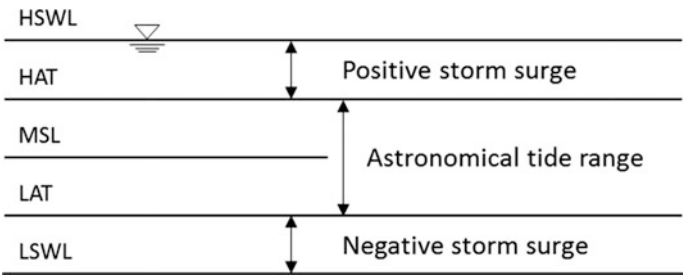

Fig. 27 Definition of water levels

Measurements and Modelling

For the design stages of a FOWT it is necessary to develop accurate and reliable site data as a basis for statistical analyses. The optimal set of data consists of long term, site-specific measurements that accurately describe the currents and sea level conditions that a FOWT would be exposed to at a particular location. However, the availability of such datasets is rare, since the time between the selection of a site and installation may only be a few years, and measurement campaigns usually only commence after a site has been selected. In this situation, hindcast data is commonly used as a supplement to establish a metocean database for a specific site. Once a metocean database has been established, the data can be statistically analysed in various ways to determine values for the metocean parameters required during the design stages.

Types of Sensors

It is important that the correct measurement instruments are used to obtain the level of information required. A thorough understanding of the instrument's measurement range, resolution and accuracy are vital to maximising the instrument's measurement potential. The instrument must also be correctly calibrated and the appropriate deployment options chosen to ensure accurate sampling of the study environment.

Currents can be measured in situ by acoustic Doppler current profilers (ADCPs) or current meters. Current meters provide a measure of flows at a fixed depth in the water column. Often numerous current meters are deployed on a single mooring and the instruments are positions at different intervals throughout the water column. ADCP are increasingly used for in situ current measurements and are capable of making non-intrusive current profile measurements through the water column. The instrument divides the measurement profile into uniform slices called depth cells and a weighted average velocity is calculated for each depth cell. ADCPs may be deployed from ship-mounted and bottom-mounted installations.

Acoustic measurement instruments measure velocity with sound, using a principle of sound waves referred to as the Doppler Effect. The instrument transmits sound at a known frequency into the water and listens for echoes of the sound reflected from particles suspended in the water. The difference between the transmitted pulse and return echo frequencies is referred to as the Doppler shift. If the particles are moving away from the instrument transducer they have a slightly lower frequency than the transmit frequency. Particles moving towards the instrument have a higher frequency. The instrument uses the difference in frequency (the Doppler shift) and the speed of sound in water to calculate the along-beam velocity i.e. the velocity of the particles (and hence the flow speed). A key assumption made by acoustic Doppler measurement instruments is that particles suspended in the water move at the same velocity as the water. ADCPs measure the radial speed of flow along the instruments inclined acoustic beams and the velocity vectors are derived from the along-beam velocity measurements. This method assumes that the flow is homogenous in the horizontal plane over the distance of separation between

the beams. For the purpose of measuring mean current velocities in tidal currents it is sufficient to use averaging periods of 10-min (DNV-RP-C205 2010).

Sea levels are typically measured at tidal stations along the coastline on a long term basis, where they can be levelled to a consistent land datum [i.e. Ordnance Datum Newlyn (ODN)]. Long-term offshore measurements of water level are not as common and more difficult because there are no obvious fixed reference points. One method of observing the offshore sea level is a pressure measuring system. The pressure at some fixed point below the sea surface is measured and converted into a level using the basic hydrostatic relationship, taking into account the water density and atmospheric pressure. Most ADCP instruments include a pressure sensor capable of measuring the water depth.

A data repository for in situ measurements of water level data across the globe is provided by the Global Sea Level Observing System (GLOSS). GLOSS is an international programme that aims to establish high quality global and regional sea level networks through a global core network of 290 sea level stations around the world (GLOSS 2016).

Measured oceanographic data are available from many stations globally and sources of data for a specific region may be identified through the Ocean Data Portal (ODP) held by the International Oceanographic and Data Information Exchange (IODE) programme of the IOC UNESCO (ODP 2016). The ODP hosts oceanographic data from a global network of 80 National Oceanographic Data Centres (NODCs). SeaDataNet and the Marine Data Exchange (by The Crown Estate in the UK) are other databases where current measurement data, as well as other oceanographic data, may be sourced for certain regions and locations. SeaDataNet is a Pan-European network that manages datasets (in situ and remote observations) for all European seas (SeaDataNet 2016). The Marine Data Exchange hosts data collated during the planning, building and operation of offshore renewable energy projects in the UK (Marine Data Exchange 2016).

Hydrodynamic Modelling

Currents and sea levels at a site can be modelled through the application of hydrodynamic models. In general, hydrodynamics models can be split into two categories: a depth averaged current model (2D) and a depth varying current model (3D). Data required to set up hydrodynamic models include the pressure and wind fields, the area bathymetry (water level) and tidal information. The more complex 3D models require additional input data, e.g. temperature, salinity and density variation over the water depth. The hydrodynamic model should be calibrated using site measurements (when available) or data from nearby locations. Another method implemented by global tide models is the assimilation of satellite altimeter data into hydrodynamic models to reduce model uncertainty (Matsumoto et al. 2000; Zijl et al. 2013). A major advantage of using satellite altimeter data is that it provides spatially well-distributed coverage of water level data, including in deep, offshore areas where measurements are less frequently available.

The hydrodynamic regime at a site is defined as the movement of a body of water driven by the actions of the tide and meteorological factors, causing changes

in the currents and sea level. Ideally, the entire sea area affecting the location should be included in the model. Often a series of progressively finer grid models may be used to achieve the required resolution of information across a site for the current and sea level conditions. The atmospheric pressure and wind data (speed and direction) are normally interpolated from a coarser model. The mean water depth is required across the site; this information may be obtained from electronically available bathymetry maps or from a dedicated bathymetric survey of the site. Tidal elevation should be specified at the model boundaries. The model calculates the surface elevation and current as a function of time in each grid point. Data produced by hydrodynamic models may be used to generate hindcast data, which can be analysed to estimate extreme current speed values (see for example Oliver et al. 2012).

Data Analysis

Prior to the analysis of measured data, high quality marine observations require quality control (QC) checks to ensure credibility and quality of the recorded data. Reference may be made to the Integrated Ocean Observing System (IOOS) manual (IOOS 2015) which reflects the present state-of-the-art in QC testing procedures for current observations. The analysis of measured currents and sea level observations has two functions. Firstly, a number of metrics can be derived from current time-series measurements to characterise the current at a development site, including current velocity and directional data with depth (from an ADCP). Secondly, measurements taken over a lunar month enable a tidal current and elevation analysis to be undertaken, which provides the basis for predicting future tides at the site. Data sets that span at least 28 days are required for a tidal analysis to determine the resolution of the primary lunar and solar constituents.

A summary of the current measurement statistic, including the principal flow direction, mean and maximum velocities, may be derived for a variety of depths to decide whether the current conditions at the site are of consequence to the FOWT design or station keeping. A histogram analysis of the processed current speeds may be completed to describe the velocity distribution at the site.

The tidal analysis of current and sea level data typically involves the decomposition of the raw time series data into a tidal and surge (residual) component. Tidal forcing is represented as a set of sinusoids at specific frequencies. Each sinusoid is referred to as a harmonic constituent that has an amplitude and phase. Harmonic analysis is the method of identifying the values of the harmonic constituent that combine to make up the tide at a specific location. The harmonic analysis process decomposes a measured velocity time series into a set of superimposed, periodic forcings, which can be used to predict the tidal current at the site in the future (or make hindcast predictions). The tidal component is deterministic and standard tidal analysis techniques may be applied to predict the tidal current and elevation for any time period over its 18.6-year nodal cycle (Pugh 1996; Pawlowicz et al. 2002). The main tidal harmonic constituents, according to Boon (2004), are: M2 (main lunar semidiurnal—period of 12.42 h); S2 (main solar semidiurnal—period of 12 h); N2 (larger lunar elliptical semidiurnal—period of

12.66 h); K1 (lunar—solar declinational diurnal—period of 23.93 h) and O1 (lunar declinational diurnal—period of 25.82 h).

Unlike deterministic tidal properties, surge events vary from event to event as small variations in weather patterns may produce variable responses in a body of water (Pugh 1996). The prediction of the non-tidal component requires a much longer dataset to reliably estimate the very low probability extreme events. Where there are insufficient observations to make statistical estimates of extreme events, hindcast data from numerical models may be used.

In practice, there are several methods of statistically modelling extreme ocean environments (Jonathan and Ewans 2013), one example is the historical method for calculating low probability values presented in ISO 19901-1 (2005). This method uses either measured or hindcast data, selects a set of the highest occurring current speeds and fits the tail of the probability distribution with an appropriate extreme distribution (i.e. Gumbel or Weibull).

3.2 Seismic Activity

The anticipated seismic activity of an area shall be assessed based on previous records of seismic events, expressed in terms of recurrence intervals and magnitude (DNV-OS-J101 2014). Information on the proximity of a site to active faults, type of faulting and sub-surface soil conditions should also be considered (ABS 2013). A Global Seismographic Network (GSN), formed in partnership with the United States Geological Survey (USGS), the National Science Foundation (NSF) and the Incorporated Research Institutions for Seismology (IRIS), provides worldwide monitoring with over 150 modern seismic stations. Data collected from the GSN are archived, and may be accessed through the IRIS data management centre (IRIS 2016). Other sources of global earthquake event data include the ISC-GEM Global Instrumental Catalogue [1900–2009] (Storchak et al. 2013) and the historical earthquake catalogue and archive [1000–1903] (Albini et al. 2013).

If a region is determined as seismically active, seismic events should be considered by taking into account the maximum ground motion that is likely to occur. Therefore the consideration of seismic events in seismically active regions shall investigate the characteristics of ground motions. Typically, actions arising from earthquakes are not of concern to the design of floating structures (ISO 19904-1 2006), however the effects of earthquake-induced foundation movements on the design of TLP-type floating support structures should be taken into account (DNV-OS-J103 2013). Details of the seismic design procedures and criteria for offshore structures can be found in ISO 19901-2 (2004).

Earthquake ground motions at a site may be described by response spectra or standardised time histories with the peak ground acceleration to characterise maximum motion (NORSOK Standard 2007). Information on the peak ground accelerations for specific annual exceedance probabilities can be found in seismic zonation maps. For example, seismic hazard estimates for the UK Continental Shelf

are presented in Health and Safety Executive (2003) and regional information for offshore areas around the globe is provided in ISO 19901-2 (2004).

In addition to seismically induced ground motions, consideration should also be given to additional seismic hazards including: tsunamis; liquefaction of subsurface soils; submarine slides; fault movement; shock waves and mud volcanoes (ISO 19901-2 2004). Tsunami waves are long with low height when travelling through deep water and pose little hazard to floating structures (ISO 19901-2 2004). A tsunami database is available from the National Oceanic and Atmospheric Administration (NOAA) in the United States, which provides information on historic tsunami events across the global (National Geophysical Data Center/World Data Service 2016). Soil investigations should be carried out to determine the dynamic soil properties and liquefaction potential at seismically active sites (ISO 19901-4 2003). Soil investigation requirements and recommendations for offshore wind turbines located in seismically active regions are given in ISO 19901-2 (2004) and DNV-OS-J101 (2014).

3.3 Ice Conditions

The relevance of sea ice conditions depends on the geographical location of the planned installation site and whether ice may develop or drift at this location. Ice conditions can pose two main threats to the durability of offshore structures, icing on the structure and the mechanical actions of sea ice (Battisti et al. 2006).

The NOAA centre host a wide variety of global ocean climatology data, including the World Ocean Database (WOD13) (Boyer et al. 2013) which presents long-term datasets of oceanographic data (i.e. temperature, salinity). Information from these global databases may provide some guidance on the relevance of ice conditions to a particular region of interest, as well as some indicative values for the relevant metocean parameters that may be suitable for conceptual studies.

Sea Ice

Sea ice is frozen ocean water, which forms and begins to grow whenever the temperature of the ocean reaches freezing point (typically −1.8 °C for seawater of salinity 32 ‰). In contrast to sea ice, icebergs, glacial and shelf ice originate on land and formed from fresh water or snow.

Sea ice can be described in terms of its thickness, its age and its movement with the wind and ocean currents. Ice types can be characterised as first-year, second-year, and multi-year sea ice, shelf ice and glacial ice. Once sea ice develops into sheet ice, it continues to thicken throughout the winter and is referred to as first-year ice. When the temperature increase in the spring the ice begins to melt, but if the ice is thick enough to remain until the following winter, it will begin to thicken again and is now referred to as second-year ice. The descriptor freezing degree-days (FDD) may be used as a measure of the general severity of ice conditions, which is related to how cold it has been for how long. The number of FDDs

during a winter is summed to calculate the frost index K (or accumulated FDD) for a winter using the following equation (ISO 19906 2010):

$$K = \left| \sum T_a - T_b \right| \tag{37}$$

where T_a is the mean daily temperature (degrees Celsius) and T_b is the freezing point of sea water.

Only days with a mean daily temperature below the freezing temperature are included. In order to calculate the actions caused by ice on a structure, values for the thickness of ice floes that are representative of the site should be defined. The ice thickness may be calculated using the frost index or an available ice atlas for the area, and used as a basis for determining design ice loads (DNV-OS-J101 2014). The frost index for a location varies from year to year and may be represented by its probability distribution, which may be used to estimate the frost index with a specified return period. The ice thickness (t) can be estimated by (DNV-OS-J101 2014):

$$t = 0.032\sqrt{0.9K - 50} \tag{38}$$

where t is in units of meters and K is the frost index in units of FDD.

Sea ice data can be obtained from direct observations, interpretation of satellite imagery or historical information available for the region of interest. NOAA provides high-resolution regional climatology information for various regions (e.g. East Asian Seas Regional Climatology (Johnson and Boyer 2015) and the Greenland, Iceland and Norwegian Seas (GINS) (Seidov et al. 2013)). On a national level, ice services (including ice charts) are typically available from national meteorological institutions.

Snow and Ice Accretion

Estimates should be made of the extent to which snow and ice may accumulate on an offshore installation. Icing on an offshore structure requires a combination of water on the offshore structure surfaces above the water level at subfreezing temperatures. Two main types of icing occur on offshore structures: atmospheric icing and icing due to sea spray.

Atmospheric icing is associated with precipitation. Super-cooling occurs in the atmosphere when the liquid phase reaches temperatures below freezing point. Super-cooled droplets can exist in several forms including freezing rain, snow, drizzle and super-cooled fog. Wet snow may freeze to the surface of a structure, but the ice formed is porous and the density of the accumulate snow (100 kg/m^3) is considerable lower than ice (900 kg/m^3) (ISO 19906 2010). Sea spray icing occurs with strong winds in combination with cold air and low sea temperatures, where sub-cooled water hits the structure and the water can freeze instantly. Sea spray is typically generated by the structure as it interacts with waves.

Icing can be measured in terms of thickness, volume or mass of ice adhering to a structure. The uneven distribution of snow or ice accretion should be considered for

buoyancy stabilised structures. Atmospheric icing may form a uniform layer of ice on all surfaces from a few meters above the sea surface, or freezing rain can potentially only cover the windward side of a surface. The ice growth process is highly dependent on both the climatic factors and the wind turbine geometry (Battisti et al. 2006).

The estimation of ice accretion on solid surfaces can be performed through direct measurement, indirect measurement or numerical modelling. Direct measurements are based on the detection of some change in physical property caused by ice accretion (e.g. ice sensors, double anemometer and vane). Indirect measurements are based on the detection of meteorological parameters that lead to icing (e.g. temperature, humidity and wind speed). The International Energy Agency (IEA) Wind Task 19 Wind Energy in Cold Climates was established to address specific issues for wind turbines operating in cold environments. Under this remit, the IEA has produced information on the state-of-the-art of wind energy in cold climates (IEA Wind Task 19, 2012) and recommended practices for wind energy projects in cold climates (IEA Wind 2012).

Acknowledgments Lucy Cradden would like to like to thank the following: The UK Met Office for permission to use data from the MIDAS dataset (© Crown Copyright, Met Office), made available via the Centre for Environmental Analysis (CEDA); Professor Gareth Harrison at the University of Edinburgh for permission to use the WRF mesoscale model data; the Global Modeling and Assimilation Office (GMAO) and the GES DISC for the dissemination of MERRA; the European Centre for Medium Range Weather Forecasting (ECMWF) for provision of ERA-40 reanalysis data.

References

References (1)

American Meteorological Society (2015) Aerodynamic roughness length. Glossary of meteorology. http://glossary.ametsoc.org/wiki/aerodynamic_roughness_length. Accessed 20 May 2015

Ayotte KW (2008) Computational modelling for wind energy assessment. J Wind Eng Ind Aerodyn 96:1571–1590

Barry R, Chorley RJ (1998) Atmopshere, weather and climate, 7th edn. Routledge, London

Barthelmie RJ, Courtney MS, Højstrup J, Larsen SE (1996) Meteorological aspects of offshore wind energy: observations from the Vindeby wind farm. J Wind Eng Ind Aerodyn 62:191–211

Burton T, Sharpe D, Jenkins N, Bossanyi E (2001) Wind energy handbook. Wiley, Chichester

Carta JA, Velázquez S, Cabrera P (2013) A review of measure-correlate-predict (MCP) methods used to estimate long-term wind characteristics at a target site. Renew Sustain Energ Rev 27:362–400

Coelingh JP, Van Wijk AJM, Holtslag AAM (1996) Analysis of wind speed observations over the North Sea. J Wind Eng Ind Aerodyn 61:51–69

Cradden L, Harrison G, Chick J (2012) Will climate change impact on wind power development in the UK? Clim Change 115:837–852

Cradden LC, Restuccia F, Hawkins SL, Harrison GP (2014) Consideration of wind speed variability in creating a regional aggregate wind power time series. Resources 3:215–234
Dee DP, Uppala SM, Simmons AJ et al (2011) The ERA-Interim reanalysis: configuration and performance of the data assimilation system. Quart J Roy Meteorol Soc 137:553–597
DNV-RP-J101 (2011) Use of remote sensing for wind energy assessments. Det Norske Veritas (DNV), Høvik, Norway
EUMETSAT (2015) Jason-2. http://www.eumetsat.int/Jason2/. Accessed 29 May 2015
Fairall CW, Grachev AA, Bedard AJ, Nishiyama RT (1996) Wind, wave, stress, and surface roughness relationships from turbulence measurements made on R/P FLIP in the SCOPE experiment. NOAA Technical Memo. ERL ETL-268. Boulder, CO, USA
Goddard Earth Sciences Data and Information Services Center (2013) MERRA reanalysis
Harrison G, Hawkins S, Eager D, Cradden L (2015) Capacity value of offshore wind in Great Britain. Proc Inst Mech Eng Part O J Risk Reliab 229(5):360–372
Hasager CB (2014) Offshore winds mapped from satellite remote sensing. Wiley Interdiscip Rev Energ Environ 3:594–603
Hasager CB, Barthelmie RJ, Christiansen MB et al (2006) Quantifying offshore wind resources from satellite wind maps: study area the north sea. Wind Energ 9(1–2):63–74
Hasager CB, Pena A, Christiansen MB et al (2008) Remote sensing observation used in offshore wind energy. IEEE J Sel Top Appl Earth Obs Remote Sens 1(1):67–79
Hawkins S (2012) A high resolution reanalysis of wind speeds over the British Isles for wind energy integration. PhD thesis, University of Edinburgh
Hess P, Brezowsky H (1952) Catalogue of european large-scale weather situations (Katalog der Großwetterlagen Europas) (in German). Bad Kissingen, Germany
IEC 61400-1 (2005) Wind turbines—Part 1: design requirements. International Electrotechnical Commission (IEC), Geneva, Switzerland
IEC 61400-3 (2009) Wind turbines—Part 3: design requirements for offshore wind turbines. International Electrotechnical Commission (IEC), Geneva, Switzerland
James PM (2007) An objective classification method for Hess and Brezowsky Grosswetterlagen over Europe. Theoret Appl Climatol 88:17–42
Kendon M, McCarthy M (2015) The UK's wet and stormy winter of 2013/2014. Weather 70 (2):40–47
Lange B, Højstrup J (2001) Evaluation of the wind-resource estimation program WAsP for offshore applications. J Wind Eng Ind Aerodyn 89:271–291
Lange B, Larsen S, Hojstrup J, Barthelmie RJ (2004) Importance of thermal effects and sea surface roughness for offshore wind resource assessment. J Wind Eng Ind Aerodyn 92:959–988
Manwell JF, McGowan JG, Rogers AL (2009) Wind characteristics and resources. In: Wind energy explained, 2nd edn. Wiley, pp 23–89
Met Office (2006a) Global marine meteorological observations data, part of the met office integrated data archive system (MIDAS). NCAS British Atmospheric Data Centre, 21 May 2015. http://catalogue.ceda.ac.uk/uuid/77910bcec71c820d4c92f40d3ed3f249
Met Office (2006b) UK mean wind data, part of the met office integrated data archive system (MIDAS). NCAS British Atmospheric Data Centre, 21 May 2015. http://catalogue.ceda.ac.uk/uuid/a1f65a362c26c9fa667d98c431a1ad38
Met Office (2011) Weather stations. http://www.metoffice.gov.uk/learning/science/first-steps/observations/weather-stations. Accessed 29 May 2015
NASA (2015) Missions: RapidScat. NASA (Jet Propulsion Laboratory). http://www.nasa.gov/rapidscat. Accessed 29 May 2015
National Data Buoy Center (2014) United States voluntary observing ship program. http://www.vos.noaa.gov/. Accessed 1 May 2015
National Data Buoy Center (2015a) National data buoy center. http://www.ndbc.noaa.gov/. Accessed 29 May 2015
National Data Buoy Center (2015b) Station 62107—sevenstones lightship. http://www.ndbc.noaa.gov/station_page.php?station=62107. Accessed 1 May 2015

Palma JMLM, Castro FA, Ribeiro LF et al (2008) Linear and nonlinear models in wind resource assessment and wind turbine micro-siting in complex terrain. J Wind Eng Ind Aerodyn 96:2308–2326
Palutikof JP, Brabson BB, Lister DH, Adcock ST (1999) A review of methods to calculate extreme wind speeds. Meteorol Appl 6:119–132
Peña A, Hasager CB, Gryning SE et al (2009) Offshore wind profiling using light detection and ranging measurements. Wind Energ 12:105–124
Petersen EL, Mortensen NG, Landberg L et al (1998) Wind power meteorology. Part I: climate and turbulence. Wind Energ 1:25–45
Plate EJ (1982) Engineering meteorology: fundamentals of meteorology and their application to problems in environmental and civil engineering. Elsevier Scientific Pub. Co, Amsterdam
Pramod Jain PD (2011) Wind resource assessment. In: Wind energy engineering. The McGraw-Hill Companies, Inc, New York
Pryor SC, Barthelmie RJ, Kjellström E (2005) Potential climate change impact on wind energy resources in northern Europe: analyses using a regional climate model. Clim Dyn 25:815–835
Rienecker MM, Suarez MJ, Gelaro R et al (2011) MERRA: NASA's modern-era retrospective analysis for research and applications. J Clim 24:3624–3648
Risien CM, Chelton DB (2006) A satellite-derived climatology of global ocean winds. Remote Sens Environ 105:221–236
Saha S, Moorthi S, Pan H-L et al (2010) The NCEP climate forecast system reanalysis. Bull Am Meteorol Soc 91:1015–1057
Sempreviva AM, Barthelmie RJ, Pryor SC (2008) Review of methodologies for offshore wind resource assessment in European seas. Surv Geophys 29:471–497
Skamarock WC, Klemp JB, Dudhia J et al (2008) A description of the advanced research WRF version 3. NCAR Techical Note
Smith DA, Harris M, Coffey AS et al (2006) Wind lidar evaluation at the Danish wind test site in Høvsøre. Wind Energ 9:87–93
Strahler AH, Strahler AN (1992) Modern physical geography, 4th edn. Wiley, New York
Stull RB (1988) An introduction to boundary layer meteorology. Springer, Netherlands
Taylor PK, Kent EC, Yelland MJ, Moat BI (1999) The accuracy of marine surface winds from ships and buoys. In: Proceedings of the CLIMAR 99, WMO workshop on advances in marine climatology, Vancouver, Canada, 8–15 Sept 1999
Troen I, Lundtang Petersen E (1989) European wind atlas. Risø Laboratory, Roskilde
Uppala SM, KÅllberg PW, Simmons AJ et al (2005) The ERA-40 re-analysis. Quart J Royal Meteorol Soc 131:2961–3012
Van Wijk AJM, Beljaars ACM, Holtslag AAM, Turkenburg WC (1990) Evaluation of stability corrections in wind speed profiles over the North Sea. J Wind Eng Ind Aerodyn 33:551–566
Watson S, Hughes J (2014) Mesoscale modelling of the UK offshore wind resource. In: Proceedings of the European wind energy association annual event. Barcelona, Spain, 10–3 Mar 2014
Weissman DE, Bourassa MA, Tongue J (2002) Effects of rain rate and wind magnitude on seawinds scatterometer wind speed errors. J Atmos Oceanic Technol 19:738–746
Wilczak JM, Oncley SP, Stage SA (2001) Sonic anemometer tilt correction algorithms. Bound-Layer Meteorol 99:127–150
World Meteorological Organization (2008) Guide to meteorological instruments and methods of observation, 7th edn. WMO-No. 8, Geneva, Switzerland, pp I.15–1 to I.15–11–II.2–10 to II.2–11

References (2)

Barstow SF, Kollstad T (1991) Field trials of the directional waverider. In: Proceedings of the 1st international offshore and polar engineering conference (ISOPE), Edinburgh, UK, 11–16 Aug 1991

Barstow S, Mørk G, Lønseth L et al (2003) WORLDWAVES: fusion of data from many sources in a user-friendly software package for timely calculation of wave statistics in global coastal waters. In: Proceedings of the 13th international offshore and polar engineering conference (ISOPE), Honolulu, Hawaii, USA, 25–30 May 2003

Barstow SF, Mørk G, Lønseth L, Mathisen JP (2009) WorldWaves wave energy resource assessment from the deep ocean to the coast. In: Proceedings of the 8th European wave and tidal energy conference (EWTEC), Uppsala, Sweden, 7–10 Sept 2009

Battjes JA (1978) Engineering aspects of ocean waves and currents. Seminar on safety of structures under dynamic loading. Trondheim, Norway

Benoit M, Frigaard P, Schaffer HA (1997) Analysing multidirectional wave spectra. In: Proceedings of the 27th IAHR congress, IAHR seminar: multidirectional waves and their interaction with structures, San Francisco, USA, 10–15 Aug 1997

Bitner-Gregersen EM, Haver S (1989) Joint long term description of environmental parameters for structural response calculation. In: Proceedings of the 2nd international workshop on wave hindcasting and forecasting, Vancouver, B.C. Canada, 25–28 Apr 1989

Bitner-Gregersen EM, Haver S (1991) Joint environmental model for reliability calculations. In: Proceedings of the 1st international offshore and polar engineering conference (ISOPE), Edinburgh, UK, 11–16 Aug 1991

Challenor PG, Foale S, Webb DJ (1990) Seasonal changes in the global wave climate measured by the Geosat altimeter. Int J Remote Sens 11(12):2205–2213

Danish Hydraulic Institute (DHI) (2015) MIKE 21 wave modelling, MIKE 21 spectral waves FM, short description. DHI, Denmark

Der-Kiureghian A, Liu P-L (1986) Structural reliability under incomplete probability information. J Eng Mech ASCE 112(1):85–104

DNV-RP-C205 (2010) Environmental conditions and environmental loads. Det Norske Veritas (DNV), Høvik, Norway

Forristal GZ (1978) On the statistical distribution of wave heights in a storm. J Geophys Res Oceans 83(C5):2353–2358

Goda Y (2000) Random sea and design of maritime structures, 2nd edn. Advanced Series on Ocean Engineering, World Scientific Publishing Company, Singapore

Guedes Soares C (1984) Representation of double-peaked spectra. Ocean Eng 11:185–207

Gunther H, Hasselmann S, Janssen PAEM (1992) The WAM model cycle 4. DKRZ technical report no. 4, Hamburg, Oct 1992

Hasselmann K (1962) On the non-linear energy transfer in a gravity-wave spectrum, Part 1: general theory. J Fluid Mech 12:481–500

Hasselmann K (1963) On the non-linear energy transfer in a gravity-wave spectrum, Part 2: conservation laws, wave-particle correspondence, irreversibility. J Fluid Mech 15:273–281

Hasselman K, Barnett TP, Bouws E et al (1973) Measurements of wind-wave growth and swell decay during the Joint North Sea Wave Project (JONSWAP). Dtsch Hydrogr Z, Suppl 12:A8

Integrated Ocean Observing System (IOOS) (2013) Manual for real-time quality control of in-situ surface wave data: a guide to quality control and quality assurance of in-situ surface wave observations, ver. 1.0. June 2013

Komen GJ, Cavaleri L, Donelan M et al (1994) Dynamics and modelling of ocean waves. Cambridge University Press, Cambridge

Krogstad HE, Barstow SF (1999) Satellite wave measurements for coastal engineering applications. Coast Eng 37:283–307

Mathiesen M, Mayer AK, Kvingedal B (2014) Hywind Buchan deep—Metocean design basis, rev. 2. Statoil document number RE2014-002, May 2014

Munk WH (1950) Origin and generation of waves. In: Proceedings of the 1st international conference on coastal engineering, long beach, California. ASCE, pp 1–4

Ochi MK, Hubble EN (1976) Six-parameters wave spectra. In: Proceedings of the 15th coastal engineering conference, Honolulu, Hawaii, USA, 1–17 July 1976

Pierson WJ, Moskowitz L (1964) A proposed spectral form for fully developed wind seas based on the similarity theory of S.A. Kitaigorodskii. J Geophys Res 69(24):5181–5190

Pontes MT, Athanassoulis GA, Barstow S et al (1996) An atlas of the wave energy resource in Europe. J Offshore Mech Arct Eng 118(4):307–309
Prince-Wright R (1995) Maximum likelihood models of joint environmental data for TLP design, In: Proceedings of the 14th international conference in offshore mechanics and arctic engineering, vol 2, ASME, New York, USA, pp 535–445
Ris RC, Holthuijsen LH, Booij N (1999) A third-generation wave model for coastal regions: 2. Verification. J Geophys Res 104(C4):7667–7681
Sarpkaya T, Isaacson M (1981) Mechanics of wave forces on offshore structures. Van Nostrand Reinhold Company, Melbourne
Smith H, Maisondieu C (2014) Resource assessment for Cornwall, Isles of Scilly and PNMI—Task 1.2 of WP3 from the MERiFIC Project: marine energy in far peripheral and island communities. MERiFIC Project, University of Exeter and Ifremer, Apr 2014
Strekalov SS, Tsyploukhin VP, Massel SR (1972) Structure of sea wave frequency spectrum. In: Proceedings of the 13th international conference on coastal engineering, vol 1. ASCE, pp 307–314
SWAN Team (2006) SWAN technical documentation, SWAN cycle III version 40.51. [Online]. Available at: www.swan.tudelft.nl. Accessed 18 Mar 2016
SWAN Team (2009) SWAN user manual, SWAN cycle III version 40.72ABCDE [Online]. Available at: www.swan.tudelft.nl. Accessed 18 Mar 2016
Torsethaugen K (1993) A two peaked wave spectrum model. In: Proceedings of the 12th international conference on offshore mechanics and arctic engineering (OMAE), Glasgow, UK, 20–24 June 1993
Tucker MJ (1993) Recommended standard for wave data sampling and near real-time processing. Ocean Eng 20:459–474
Tucker MJ, Pitt EG (2001) Waves in ocean engineering. In: Bhattacharyya R, McCormick ME (eds) Elsevier ocean engineering series, vol 5. Elsevier Science & Technology, Oxford
WAMDI Group (1988) The WAM model—a third generation ocean wave prediction model. J Phys Oceanogr 18(12):1775–1810
Winterstein S, Ude TC, Cornell CA et al (1993) Environmental parameters for extreme response: inverse FORM with omission sensitivity. In: Proceedings of the ICOSSAR-93, Innsbruck, Austria, 9–13 Aug 1993
Young IR (1999) Wind generated ocean waves. In: Bhattacharyya R, McCormick ME (eds) Elsevier ocean engineering series, vol 2. Elsevier Science & Technology, Oxford

References (3)

Albini P, Musson RMW, Gomez Capera AA et al (2013) Global historical earthquake archive and catalogue (1000-1903). GEM technical report 2013-01 V1.0.0, GEM Foundation, Pavia, Italy
American Bureau of Shipping (ABS) (2013) Guide for building and classing floating offshore wind turbine installations. ABS Guideline #195. Houston, TX, USA
Battisti L, Fedrizzi R, Brighenti A, Laakso T (2006) Sea ice and icing risk for offshore wind turbines. In: Proceedings of the OWEMES 2006, Civitavecchia, Italy, 20–22 Apr 2006
Boon J (2004) Secrets of the tide: tide and tidal current analysis and predictions, storm surges and sea level trends. Horwood Publishing Ltd, Chichester
Boyer TP, Antonov JI, Baranova OK et al (2013) World ocean database 2013. NOAA Atlas NESDIS 72, Ed. Levitus S, Technical Ed. Mishonov A. Silver Spring, MD, USA, 209 pp
DNV-OS-J101 (2014) Design of offshore wind turbine structures. Det Norske Veritas (DNV), Høvik, Norway
DNV-OS-J103 (2013) Design of floating wind turbine structures. Det Norske Veritas (DNV), Høvik, Norway
DNV-RP-C205 (2010) Environmental conditions and environmental loads. Det Norske Veritas (DNV), Høvik, Norway

GLOSS (2016) GLOSS station handbook. http://www.gloss-sealevel.org/station_handbook/. Accessed 28 Mar 2016
Health and Safety Executive (2003) An appraisal of existing seismic hazard estimates for the UK continental shelf. Research report 166. ISBN 0 7176 2778 0
IEA Wind (2012) Expert group study on recommended practices, 13. Wind energy projects in cold climates, edn 1. International Energy Agency, May 2012
IEA Wind Task 19 (2012) State-of-the-art of wind energy in cold climates. International Energy Agency, Oct 2012
IEC 61400-3 (2009) Wind turbines—part 3: design requirements for offshore wind turbines. International Electrotechnical Commission (IEC), Geneva, Switzerland
Integrated Ocean Observing System (IOOS) (2015) Manual for real-time quality control of in-situ current observations: a guide to quality control and quality assurance of acoustic Doppler current profiler observations, Version 2.0. Oct 2015
IRIS (2016) IRIS earthquake browser, incorporated reasearch institutions for seismology (IRIS). http://ds.iris.edu/ieb. Accessed 28 Mar 2016
ISO 19901-1 (2005) Petroleum and natural gas industries—specific requirements for offshore structures part 1: Metocean design and operating considerations. International Organization for Standardization (ISO), Geneva, Switzerland
ISO 19901-2 (2004) Petroleum and natural gas industries—specific requirements for offshore structures part 2: seismic design procedures and criteria. International Organization for Standardization (ISO), Geneva, Switzerland
ISO 19901-4 (2003) Petroleum and natural gas industries—specific requirements for offshore structures part 3: geotechnical and foundation design considerations. International Organization for Standardization (ISO), Geneva, Switzerland
ISO 19904-1 (2006) Petroleum and natural gas industries—floating offshore structures and mobile offshore units. International Organization for Standardization (ISO), Geneva, Switzerland
ISO 19906 (2010) Petroleum and natural gas industries—artic offshore structures. International Organization for Standardization (ISO), Geneva, Switzerland
Johnson DR, Boyer TP (2015) Regional climatology of the East Asian seas: an introduction. NOAA Atlas NESDIS 79. Silver Spring, MD, USA, pp 37
Jonathan P, Ewans K (2013) Statistical modelling of extreme ocean environments for marine design: a review. Ocean Eng 62:91–109
Marine Data Exchange (2016) Marine data exchange. The crown estate. http://www.marinedataexchange.co.uk/. Accessed 28 Mar 2016
Matsumoto K, Takanezawa T, Ooe M (2000) Ocean tide models developed by assimilating TOPEX/POSEIDON altimeter data into hydrodynamical model: a global model and a regional model around Japan. J Oceanogr 56:567–581
National Geophysical Data Center/World Data Service (NGDC/WDS) (2016) Global historical tsunamic database. National Geophysical Data Center, NOAA. doi:10.7289/V5PN93H7. Accessed 28 Mar 2016
NORSOK Standard (2007) N-003 action and action effects, edn 2. Sept 2007
Ocean Data Portal (2016) Ocean data portal. http://www.oceandataportal.org/. Accessed 28 Mar 2016
Oliver EC, Sheng J, Thompson KR, Urrego Blanco JR (2012) Extreme surface and near-bottom currents in the northwest Atlantic. Nat Hazards 64:1425–1446
Pawlowicz R, Beardsley B, Lentz S (2002) Classical tidal harmonic analysis including error estimates in MATLAB using T TIDE. Comput Geosci 28:929–937
Pugh DT (1996) Tides, surges and mean sea-level (reprinted with corrections). Wiley, Chichester
SeaDataNet (2016) SeaDataNet. Pan-European infrastructure for ocean and marine data management. http://www.seadatanet.org/. Accessed 28 Mar 2016
Seidov D, Baranova OK, Biddle M et al (2013) Greenland-Iceland-Norwegian seas regional climatology, Regional Climatology Team. NOAA/NCEI

Storchak DA, Di Giacomo D, Bondár I et al (2013) Public release of the ISC-GEM global instrumental earthquake catalogue (1900-2009). Seismol Res Lett 84(5):810–815

Zijl F, Verlaan M, Gerritsen H (2013) Improved water-level forecasting for the Northwest European Shelf and North Sea through direct modelling of tide, surge and non-linear interactions. Ocean Dyn 63:823–847

Springer

http://www.springer.com/978-3-319-29396-7

Floating Offshore Wind Energy
The Next Generation of Wind Energy
Cruz, J.; Atcheson, M. (Eds.)
2016, VII, 341 p. 168 illus., 107 illus. in color.,
Hardcover
ISBN: 978-3-319-29396-7